12

(6) SMALL SCALE DISCHARGE STUDIES.

(10) J. A. Mangano, M. Rokni, J. H. Jacob and J. C. Hsia
Avco Everett Research Laboratory, Inc.
2385 Revere Beach Parkway
Everett MA 02149

(9) Semi-Annual Report, for Period 1 March 1977 to 31 August 1977,

(11) 31 Aug 77 (12) 89 p.

(15) N0014-75-C-0062, ARPA Order-1806

Sponsored by
DEFENSE ADVANCED RESEARCH PROJECTS AGENCY
DARPA Order No. 1806

Monitored by
OFFICE OF NAVAL RESEARCH
DEPARTMENT OF THE NAVY
Arlington VA 22217

FOREWORD

DARPA Order No.: 1806

Program Code No.: 5E20

Name of Contractor: Avco Everett Research Laboratory, Inc.

Effective Date of Contract: 15 August 1974

Contract Expiration Date: 15 November 1977

Amount of Contract: $1,283,451

Contract No.: N00014-75-C-0062

Principal Investigator and Phone No.: J.H. Jacob
(617) 389-3000, Ext. 329

Scientific Officer: Director, Physics Program, Physical Sciences Div.
Office of Naval Research
Department of the Navy
800 North Quincy Street
Arlington, VA 22217

Short Title of Work: Laser Discharge Studies

UNCLASSIFIED

SECURITY CLASSIFICATION OF THIS PAGE (When Data Entered)

REPORT DOCUMENTATION PAGE		READ INSTRUCTIONS BEFORE COMPLETING FORM
1. REPORT NUMBER	2. GOVT ACCESSION NO.	3. RECIPIENT'S CATALOG NUMBER
4. TITLE (and Subtitle) SMALL SCALE DISCHARGE STUDIES		5. TYPE OF REPORT & PERIOD COVERED Semi-Annual Report 1 March 1977 to 31 Aug. 1977 6. PERFORMING ORG. REPORT NUMBER
7. AUTHOR(s) J.A. Mangano, M. Rokni, J.H. Jacob and J.C. Hsia		8. CONTRACT OR GRANT NUMBER(s) N00014-75-C-0062
9. PERFORMING ORGANIZATION NAME AND ADDRESS Avco Everett Research Laboratory, Inc. 2385 Revere Beack Parkway Everett, MA 02149		10. PROGRAM ELEMENT, PROJECT, TASK AREA & WORK UNIT NUMBERS
11. CONTROLLING OFFICE NAME AND ADDRESS Defense Advanced Research Projects Agency DARPA Order No. 1806		12. REPORT DATE 13. NUMBER OF PAGES 80
14. MONITORING AGENCY NAME & ADDRESS(if different from Controlling Office) Office of Naval Research Department of the Navy Arlington, VA 22217		15. SECURITY CLASS. (of this report) Unclassified 15a. DECLASSIFICATION/DOWNGRADING SCHEDULE

16. DISTRIBUTION STATEMENT (of this Report)

Approved for Public Release; Distribution Unlimited.

17. DISTRIBUTION STATEMENT (of the abstract entered in Block 20, if different from Report)

18. SUPPLEMENTARY NOTES

19. KEY WORDS (Continue on reverse side if necessary and identify by block number)

20. ABSTRACT (Continue on reverse side if necessary and identify by block number)

In this article the rare gas fluoride lasers are discussed in detail. There is a significant interest in these lasers because they are the most efficient visible/UV lasers to date. The dominant formation kinetics of KrF^* and XeF^* in both discharges and e-beam pumped lasers are presented. Because of the ionic upper level the formation processes are rapid and conditions can be chosen such that the branching ratio into the KrF^* and XeF^* levels from both the ionic and metastable levels are unity. In e-beam pumping, a guide magnetic field

DD FORM 1 JAN 73 1473 EDITION OF 1 NOV 65 IS OBSOLETE

UNCLASSIFIED

SECURITY CLASSIFICATION OF THIS PAGE (When Data Entered)

(20)

enables the deposition of 70% of the beam energy into the optical volume. If two e-beams can be used > 90% of the fast electron energy can be deposited into the optical volume. Discharge pumping has the potential of being more efficient than e-beam however, key technical issues of discharge stability, and metastable production efficiency have to be addressed. Stabilization of the discharge appears possible if an external source of ionization is used. The quenching of the rare gas fluorides by two or three body processes have been carefully measured and analyzed. The three body quenching of KrF^* leads to the eventual formation of the excited triatomic Kr_2F^* which radiates in a broad band centered at 410 mm. We have also determined that ionic and excited state absorption in the active media are large enough to impact the extraction efficiency of these lasers. In the case of KrF^* the dominant absorbing species are F_2, F^- and Kr_2F^*, while Xe_2^+ appears to be the dominant absorber in XeF^*. Finally, we have also investigated experimentally and theoretically the effects of the vibrational relaxation in the upper level and finite lifetime of the lower level on the XeF^* laser performance.

REPORT SUMMARY

In this semi-annual report, we review and summarize the research conducted on the small scale discharge studies during the last two years. Emphasis, of course, has been placed on the more recent results. The dominant formation kinetics of the KrF^* and XeF^* lasers are discussed in detail. Both e-beam pumping and discharge pumping have been considered. The discharge has the potential of being more efficient. However, key technical issues have to be resolved (a) discharge stability, (b) discharge enhancement and (c) metastable production efficiency. These issues were intensively investigated on the small scale and meter device. Unfortunately, in the meter device, if most of the e-beam ionization is to be used, non-uniformities in the ionization rate results in a volumetric unstable discharge. The quenching kinetics has also been fully investigated. In KrF^*, we discovered that three body quenching led to the eventual formation of the excited triatomic Kr_2F^*. The active media absorption of both KrF^* and XeF^* have been thoroughly researched. The dominant absorbing species in KrF^* is F_2, F^- and Kr_2F^*, while Xe_2^+ is the dominant absorber in XeF^*. Finally, the impact of the upper vibrational relaxation and finite lifetime of the lower laser level on the XeF^* laser performance was investigated both experimentally and theoretically.

TABLE OF CONTENTS

LIST OF ILLUSTRATIONS

I. INTRODUCTION

Rare gas fluoride exciplexes are the most efficient visible/UV lasers to date. The rare gas monohalide lasers have been actively investigated since their emission spectra was reported three and half years ago by Velazco and Setser[1] and by Golde and Thrush.[2] Table 1 lists the exciplexes that have been made to lase and the method by which they were excited. $XeBr^*$ was the first of this class to lase. This molecule was excited by a relativistic electron beam by Searles and Hart.[3] Shortly after that Ewing and Brau[4, 5] obtained lasing action in XeF^*, $XeC\ell^*$ and KrF^*. Recently a new family of lasers, mercury monohalides, have been demonstrated by J. H. Parks.[6] Lasing action of the mercury monohalides was first predicted by J. J. Ewing.[7] As one can see from Table 1 all the exciplexes have been made to lase by relativistic e-beam pumping, indicating that this is the easiest way to obtain stimulated emission. The best results obtained by pure e-beam pumping[8] for a KrF^* laser are 12 J/liter and 9% intrinsic efficiency.

---

(1) J. E. Velazco and D. W. Setser, "Quenching of Xe Metastable Atoms," JQE 11, 708-709 (1975).

(2) M. C. Golde and B. A. Thrush, Chem. Phys. Lett. 29, 486 (1974).

(3) S. K. Searles and G. A. Hart, "Stimulated Emission at 281.8 nm from XeBr," Appl. Phys. Lett. 27, 243-245 (1975).

(4) J. J. Ewing and C. A. Brau, "Laser Action on the $^2\Sigma^+_{1/2} \rightarrow {}^2\Sigma^+_{1/2}$ Bands of KrF and $XeC\ell$," Appl. Phys. Lett. 27, 350-352 (1975).

(5) C. A. Brau and J. J. Ewing, "354 nm Laser on XeF," Appl. Phys. Lett. 27, 435-437 (1975).

(6) J. H. Parks, "Laser Action on the $B^2\Sigma^+_{1/2} \rightarrow X^2\Sigma^+_{1/2}$ Band of $HgC\ell$ at 5576 Å," Appl. Phys. Lett. 31, 192-194 (1977).

(7) J. J. Ewing, private communication (1976).

(8) J. A. Mangano and J. Hsia, "Interim Report-One Meter KrF^* Laser," Semi-Annual Technical Report Aug 76 - Feb 77.

TABLE 1. CANDIDATE LASER MOLECULES

EXICPLEX	WAVELENGTH nm	E-BEAM PUMPING	DISCHARGE PUMPING	
			E-BEAM CONTROLLED	AVALANCHE
XeBr	282	X		
XeCl	308	X		
XeF	352	X	X	X
KrCl	222	X		
KrF	249	X	X	X
ArF	192	X		X
HgCl	558	X	X	
HgBr	502	X		

H1585

Pumping of the rare gas monohalide lasers with an e-beam controlled discharge was first demonstrated by Mangano and Jacob.[9] In e-beam controlled discharge pumping a discharge voltage is applied across the mixture which is ionized by an e-beam. This method has the potential of being more efficient than pure e-beam pumping. However, to achieve this, key technical issues of discharge stability and discharge enhancement have to be resolved. The best results[10] to date by this method of puming is 10 J/liter with an intrinsic efficiency of 9.5%, obtained in a KrF^* laser. The third method of exciting these lasers is the UV-preionized discharge.[11, 12] This is the simplest system to build; however, the efficiency is limited to about one percent. In this method ultraviolet light is used to preionize the medium followed by an avalanche discharge. An avalanche discharge yields higher pulse-repetition rates and is simpler than other pump methods. Its potential applications are isotope separation and other photochemical processes which require pulses of one joule or less. Avalanche pumping lacks the control of e-beam ionized discharges and so the power and pulse lengths attainable are limited as will be discussed in the text. The controlled-discharge technique gives much higher energy per pulse and has the potential of being scaled to higher average power than the avalanche approach. This is because in a stable discharge long laser pulses with higher efficiency are possible.

(9) J. A. Mangano and J. H. Jacob, "E-Beam Controlled Discharge Pumping of the KrF^* Laser," Appl. Phys. Lett. 27, 495-498 (1975).

(10) J. A. Mangano and J. Hsia, Interim Report - One Meter KrF^* Laser," Semi-Annual Technical Report Feb 77 - Aug 77.

(11) R. Burnham, H. W. Harris and N. Djeu, "Xenon Fluoride Laser Excitation by Transverse Electric Discharge," Appl. Phys. Lett. 28, 86-87 (1976).

(12) C. P. Wang, H. Mirels, D. G. Sutton and S. N. Suchard, "Fast Discharge Initiated XeF Laser," Appl. Phys. Lett. 28, 326-328 (1976).

To build an efficient laser the following criteria have to be met. (1) the formation efficiency of the upper laser level must be high; the formation efficiency is the product of the branching ratio and quantum efficiency; (2) the quenching of the upper laser level should not be extremely rapid; (3) the absorption of the active media should be small to enable efficient optical extraction; and (4) the lower laser level should be removed rapidly. To date, the lasers that have shown the most promise are the rare gas fluorides which have high formation efficiencies, both by e-beam[13, 14] and e-beam controlled discharge pumping.[15] In this report we will discuss in detail the physics of the KrF^* lasers which are proto-typical of efficient exciplex lasers. The main difference between KrF^* and XeF^* is that KrF^* has an unbound lower level while XeF^* is bound by about 0.15 eV. The fffects of the bound lower level on the laser performance will be discussed subsequently. We will show the extent to which the above criteria are satisfied by these lasers.

In Figure 1 we see a schematic potential diagram of a rare gas halide exciplex. There are two noteworthy features: (a) the upper level correlates with a $R^+ + X^-$ ion pair where R^+ denotes a rare gas ion and X^- a halogen ion; and (b) the lower level is in most cases unbound. The laser transitions are characterized by large stimulated cross-section (1 - 5 $Å^2$) and short radiative lifetimes (5 - 15 nsec). The ionic nature of the upper level allows for rapid formation via both the ionic[13, 14] and metastable

---

(13) J. A. Mangano, J. H. Jacob, M. Rokni and A. Hawryluk, "Three Body Quenching of KrF^* by Ar and Broadband Emission at 415 nm," Appl. Phys. Lett. 31, 26-28 (1977).

(14) M. Rokni, J. H. Jacob, J. A. Mangano and R. Brochu, "Two and Three Body Quenching of XeF^* by Ar and Xe," Appl. Phys. Lett. 30, 458-460 (1977).

(15) J. H. Jacob and J. A. Mangano, "Modeling of the KrF Laser Discharge," Appl. Phys. Lett. 28, 724-726 (1976).

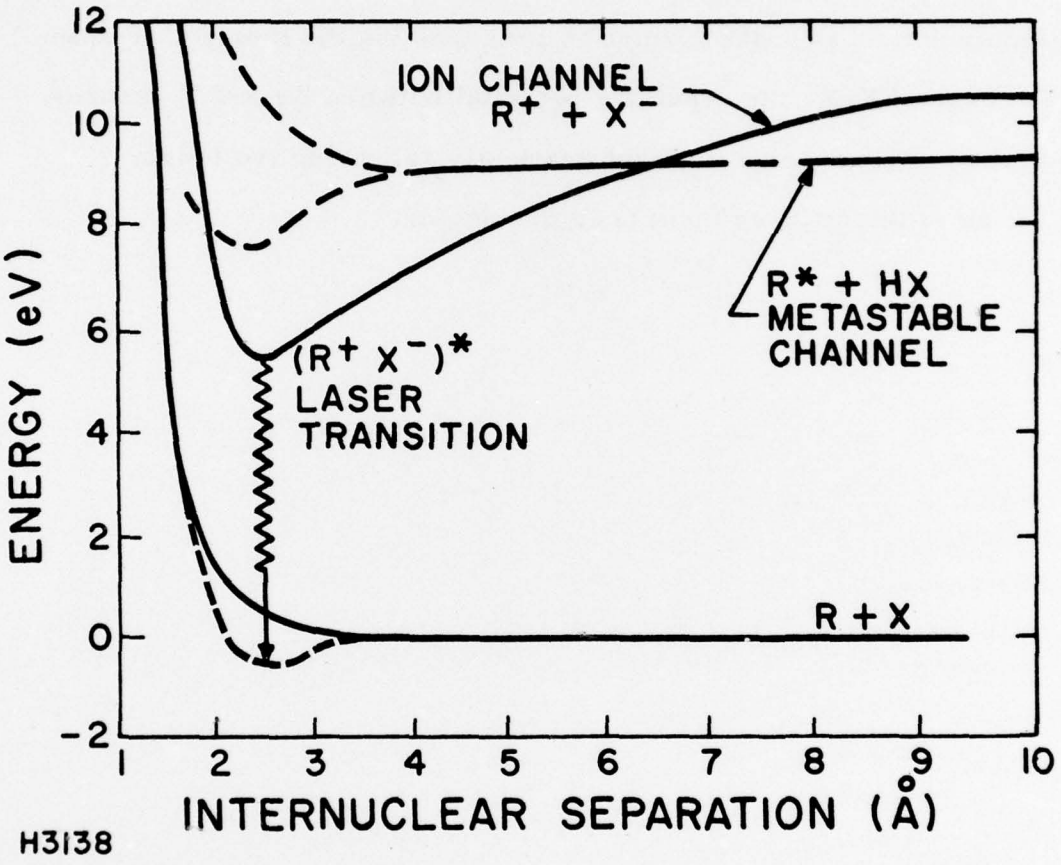

Figure 1 Typical Potential Energy Diagram of a Rare Gas Fluoride

channels.[1] In most rare gas fluorides there are only a few curve crossings with excited molecular levels. As a result, the probability of interception is small and the formation efficiency is high. The ionic channel is usually dominant in pure e-beam pumping (see Figure 1), while in e-beam controlled discharge pumping most of the formation proceeds via the metastable channel. In the case of KrF^* the repulsive potential between Kr and F ensures a negligible lower level population automatically satisfying the fourth criteria for an efficient laser mentioned previously.

II. FORMATION KINETICS

A. E-BEAM PUMPED KrF^*

Typical mixtures contain about 90% Ar, $\leq 0.5\%$ F_2 at a total pressure of 1 - 3 atm. Figure 2 shows schematically the dominant formation kinetics. Since the mixture contains mainly Ar, most of the e-beam power deposited results in argon ion-electron pairs. For typical current densities of 5-10 A/cm^2, the dominant loss of secondary electrons is rapid dissociative attachment with F_2 resulting in F^- formation. At higher current densities, electron, molecular ion recombination (Ar_2^+) becomes more important, resulting in rare gas metastable formation. At pressures below an atmosphere, the Ar^+ and F^- recombine to form ArF^*. The ArF^* can radiate at 193 nm and form ground state Ar and F atoms. The radiative lifetime has been calcalculated to be about 4 nsec. However, for mixtures containing > 5% krypton[13] and mixture pressures > 1/2 atmosphere, the Kr will exchange efficiently with the ArF^* to form KrF^*. At pressure above an atmosphere, the Ar^+ and Ar react predominantly to form Ar_2^+ with a threebody rate of 2.5×10^{-31} $cm^6/sec.$[16] The Ar_2^+ then undergoes charge transfers with Kr to form Kr^+ with a rate constant of 7.5×10^{-10} $cm^3/sec.$[17] For lean Kr mixtures

---

(16) E.W. McDaniel, V. Cermak, A. Dalgarno, E.E. Ferguson and L. Friedman, "Ion-Molecule Reactions," (Wiley-Interscience, New York, 1970) pp. 338-339.

(17) D.K. Bohme, N.G. Adams, M. Moselman, D.B. Dunking and E.E. Ferguson, "Flowing Afterglow Studies of the Reactions of the Rare-Gas Molecular Ions He_2^+, Ne_2 and Ar_2^+ with Molecules and Rare-Gas Atoms," J. Chem. Phys. 52, 5094 (1970).

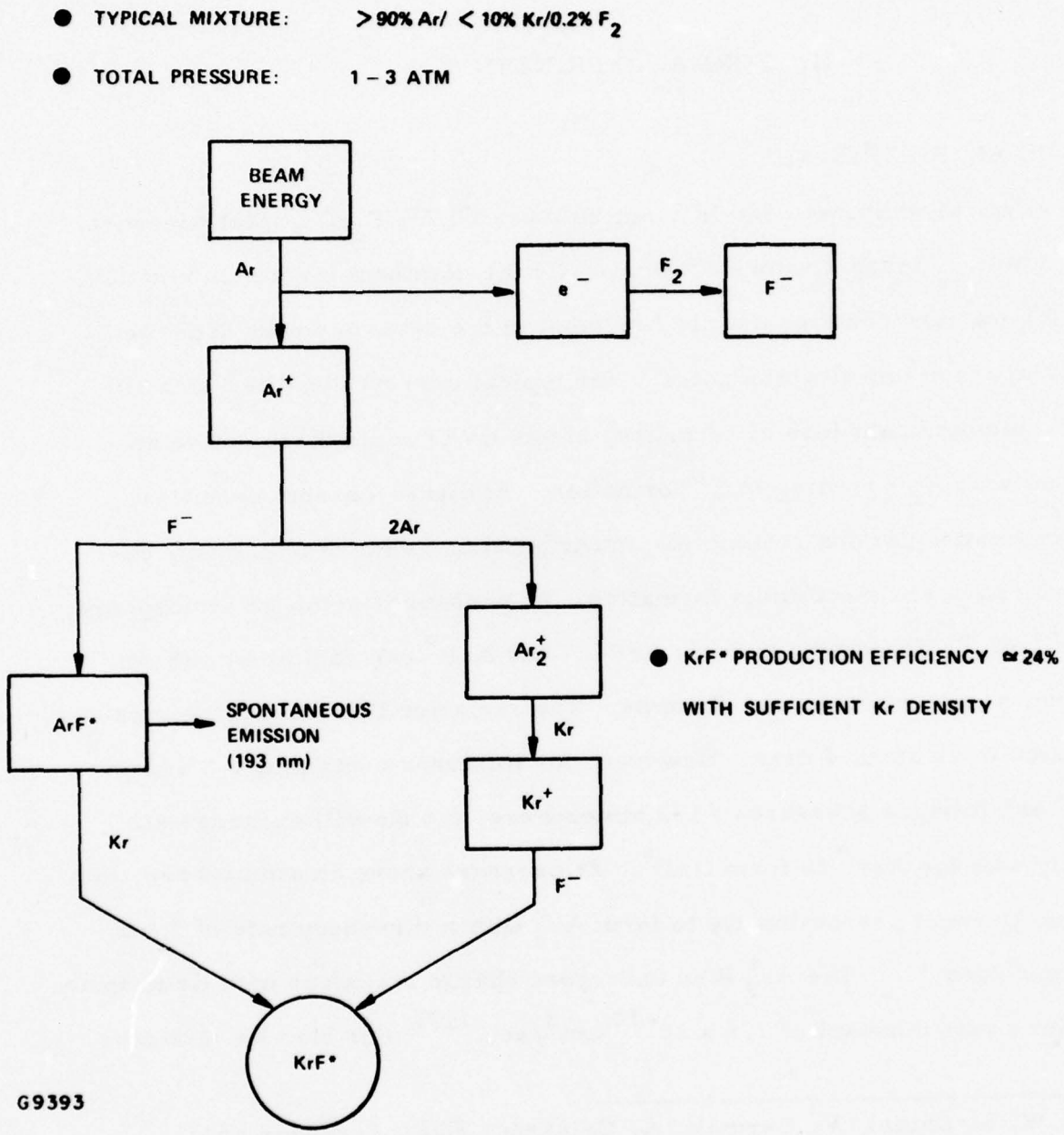

Figure 2 Dominant Formation Kinetics of E-Beam Pumped KrF*

the Kr^+ will combine with the F^- to form KrF^*. As the Kr number density is increased (or the total mixture pressure), molecular krypton ion are formed. These ions also combine with F^- to form mainly KrF^*.[13] The KrF^* can spontaneously decay with a lifetime of 6.5 nsec[18] or can be collisionally quenched. The quenching process will be discussed subsequently.

B. E-BEAM PUMPED XeF

Typical mixtures contain about $\leq$ 0.5% NF_3, $\leq$1% Xe and the remainder is Ar or Ne. The formation kinetics in Ar-rich XeF^* mixtures is similar to KrF^* which has been discussed previously. In XeF^* laser mixtures NF_3 is used instead of F_2. The main advantage of using NF_3 is that it does not absorb the XeF^* laser radiation.[19] The details of the formation processes with Ne are not well established; however, experimental results indicate that the branching into XeF^* in Ne-diluted mixtures is the same within experimental error as in Ar-diluted mixtures. This conclusion was arrived at by comparing the fluorescence intensity of $Ne/Xe/F_2$ mixtures with that of similar $Ar/Xe/F_2$ mixtures (from 1/2-4 atm).[20] In making this comparison we have accounted for the difference in the e-beam stopping power, the energy required to create an electron/ion pair, and the different quenching rates of XeF^* for the different mixtures.

The fluorescence spectra for typical $Ar/Xe/F_2$ and $Ne/Xe/F_2$ mixtures are shown in Figure 3. This data was taken at total mixture pressure of 3 atm and contained 0.3% F_2 and 0.5% of Xe. From the spectra in Figure 3,

(18) Thom H. Duning and P. Jeffery Hay, "Electronic States of KrF," Appl. Phys. Lett. 28, 649-651 (1976).

(19) S.R. LaPaglia and A.B.F. Duncan, J. Chem. Phys. 34, 1003 (1961).

(20) M. Rokni, J.H. Jacob and J.A. Mangano, "Formation Processes in E-beam Pumped $Ne/Xe/F_2$ Mixtures," Appl. Phys. Lett. to appear in Feb. (1978).

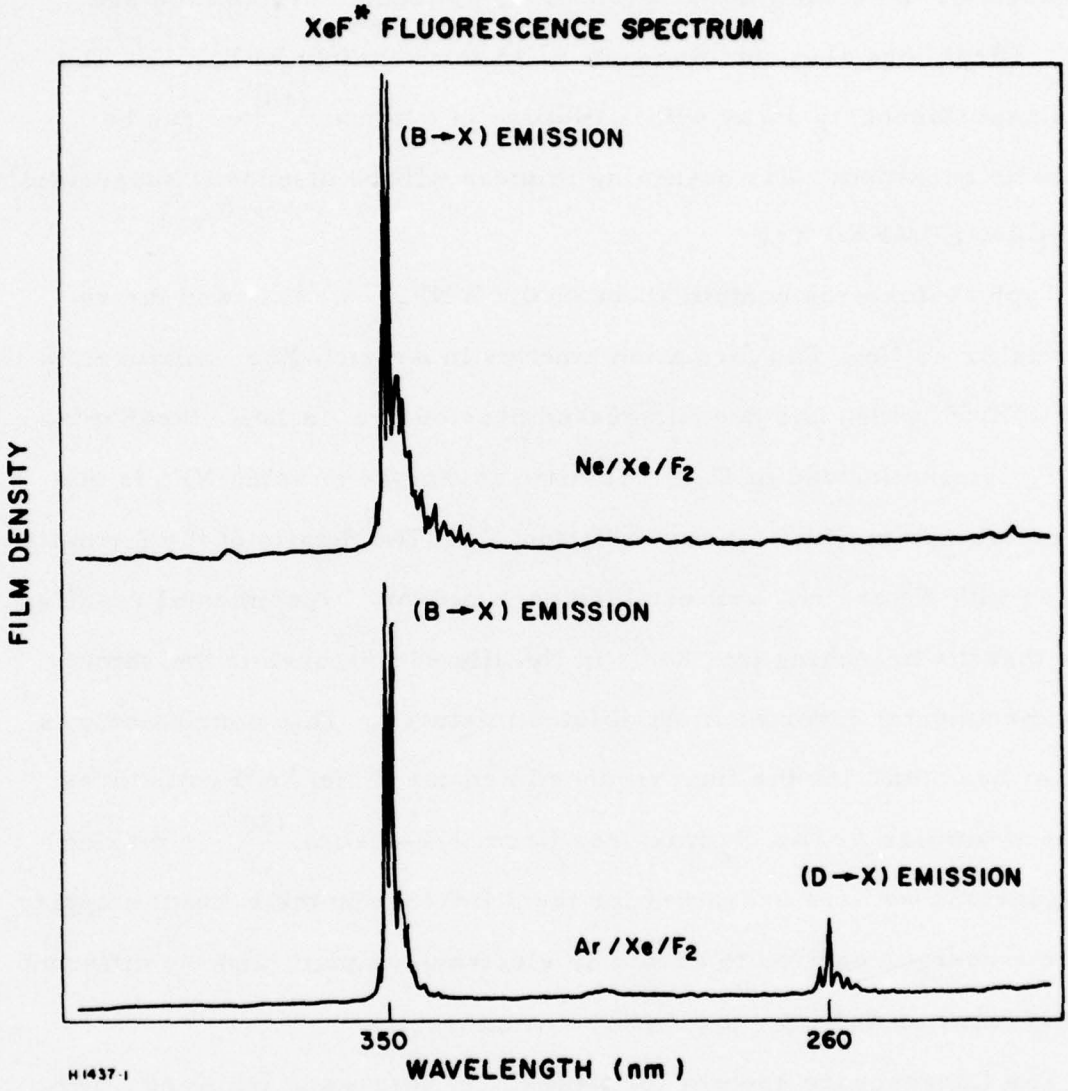

Figure 3 Comparison Between Emission Spectra of $Ar/Xe/F_2$ and $Ne/Xe/F_2$ Mixtures. The mixtures contain 0.3% F_2, 0.5% Xe at a total pressure of 3 atm.

one sees two differences between the Ne and Ar-diluted mixtures, i.e., (a) the XeF^* (D→X) emission at 260 nm is present only in the $Ar/Xe/F_2$ excited mixture, and (b) the (B→ X) emission in the Ne-rich mixture is broader than in the Ar-rich mixture. The D state correlates with the Xe^+ ($^2P_{1/2}$) while the B state correlates with the Xe^+ ($^2P_{3/2}$) states.[21] These differences were present in all spectra obtained in the pressure range between 0.5 - 3 atm. The greatly reduced intensity of the D → X emission in Ne-rich mixtures is because the Xe^+ ($^2P_{1/2}$) is not created in these mixtures, even though Ne_2^+ has sufficient energy to charge transfer to Xe^+($^2P_{1/2}$) and Xe^+ ($^2P_{3/2}$). This implies that Ne_2^+ charge transfer to Xe^+ is not a dominant formation process of XeF.[22] Also, NeF^* has 11.6 eV of energy[23] which is larger by 3 eV than the $Xe^+ + F^-$ energy at infinite separation. So there is no curve crossing and it is unlikely that the Ne atom in NeF^* will be displaced by Xe to form XeF^*.

A possible formation chain that is consistent with experimental observations is shown in Figure 4. Since Ne is the major species in the mixture, NeF^* will be formed by reaction of Ne^+ and Ne_2^+ with F^-.[21] Once NeF^* is formed, it can spontaneously radiate or predissociate to F^* and Ne. The predissociation of NeF^* is expected because atomic fluorine has an

---

(21) Dunning & Hay, LASL, private communication.

(22) Measurements by D.K. Bohme, N.C. Adams, M. Muselman, D.B. Dunking and E.E. Ferguson, in Ref. 17 show that the rate constant for $Ne_2^+ + K_r \rightarrow Kr^+ + 2\ Ne$ and $Ne_2^+ + Ar \rightarrow Ar^+ + 2\ N_e$ is very slow ($< 5 \times 10^{-13}$ cm^3/sec). So it is reasonable to expect that the charge transfer from $Ne_2^+ \rightarrow X_e^+$ will not be dominant in e-beam pumped XeF laser mixtures.

(23) C.A. Brau and J.J. Ewing, "Emission Spectra of XeBr, XeCℓ, XeF and KrF^*," J. Chem. Phys., 63, 4640-4647 (1975).

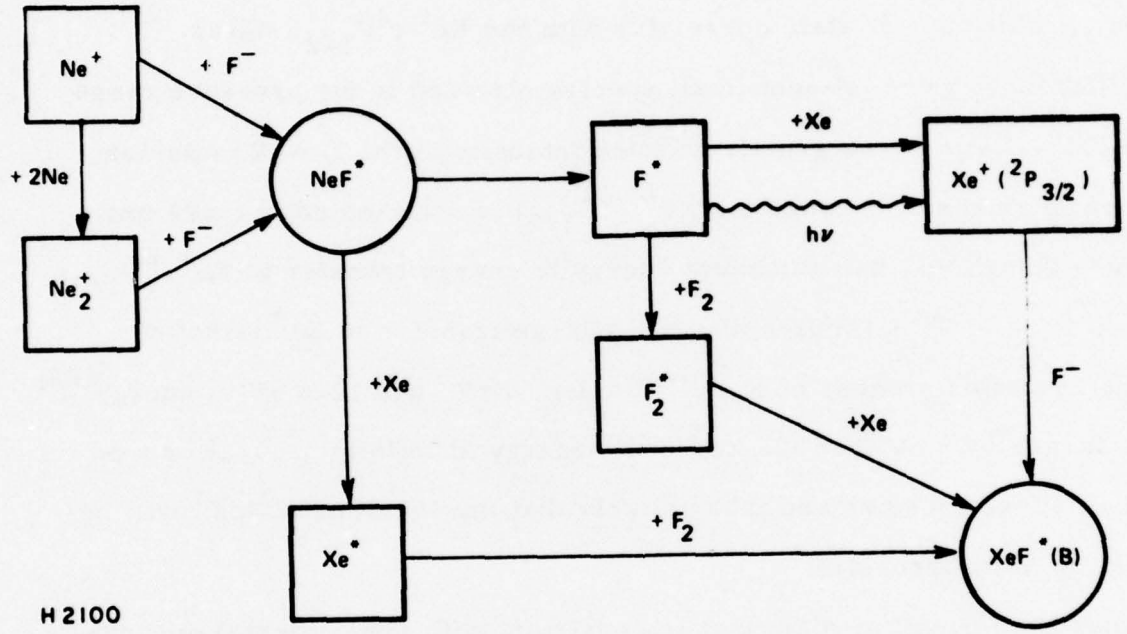

Figure 4 Possible XeF* Formation Processes in E-Beam Pumped Ne/Xe/F_2 Mixtures

ensemble of levels (^4P and ^2P) about 1 eV above the bottom of the NeF^* well.[24] NeF^* can also collisionally excite Xe to high lying excited levels which will eventually form XeF^*. The F^* which is produced by the NeF^* predissociation can radiate, Penning ionize Xe, or form F_2^* by reaction with F_2. F^* is energetic enough to ionize Xe to the $^2P_{3/2}$ level only. Also, the radiated photons from F^* can photoionize Xe. The cross section for this process is 6×10^{-17} cm^2,[29] resulting in a photoabsorption length of 1.5 mm in a 0.5% Xe mixture at a total pressure of one atmosphere. The F_2^* can react with Xe in a harpoon-like reaction to form XeF^*. Al the above kinetic processes will produce XeF(B) and not XeF(D).[23] Hence, the $D \rightarrow X$ emission at 260 nm is not observed in Ne-rich mixtures as shown in Figure 3.

The broader emission on the $(B \rightarrow X)$ band of XeF^* with a Ne buffer (compared to Ar) indicates that the vibrational relaxation in the XeF(B) manifold by Ne is slower than that by Ar. Since Ne is lighter than Ar, relaxation by V-T transfer would proceed more rapidly in Ne-rich mixtures. So it appears that V-T energy transfer is not a dominant process. A possible explanation is that Ar and Xe can form a molecular ion $ArXe^+$ whereas $NeXe^+$ is more weakly bound.[26] Hence, an intermediate complex $ArXeF^*$ can be formed which will result in a more rapid vibrational relaxation of XeF^*.[23] The formation of such complexes may also explain why Ar quenches XeF^* more rapidly than Ne.

---

(24) M. Krauss, NBS, private communication.

(25) J.A.R. Samson and K.L. Kelly, C.C.A. Tech. Rept. No. 69-3-N (1964)

(26) M. Krauss, NBS, private communication.

C. DISCHARGE PUMPED KrF^*

The gas mixtures for discharge pumping and e-beam pumping of KrF^* are similar. For efficient discharge pumping the formation should proceed via the metastable channel. Figure 5 shows schematically the dominant formation kinetics.

In e-beam controlled discharge pumping the secondary electrons gain enough energy in an applied electric field to excite the argon and krypton metastables. The argon metastables, Ar^*, produces ArF^* with a branching ratio of about 0.6[27] via the harpoon reaction with F_2 ($Ar^* + F_2 \rightarrow ArF^* + F$). The rate constant for this reaction has been measured by Velacazo, Kolts and Setser to be 7.8×10^{-10} cm^3/sec.[30] As we have discussed previously the ArF^* can either radiate or the Ar atom can be displaced by the Kr to form KrF^*. The krypton metastable Kr^* can form KrF^* directly, and with a branching ratio of unity, via the harpoon reaction with F_2.[27] Because of the lower energy required to excite Kr^* and the unit branching ratio to form KrF^*, the formation efficiency will be larger if most or all the discharge energy goes into Kr^*. The fraction of discharge energy that is deposited into Kr^* will depend on the percentage of Kr and applied electric field as shown in Figure 6. Clearly, the higher the fraction of Kr, the larger the formation efficiency. However, as we will show subsequently, Kr quenches KrF^* more rapidly and hence the fraction of Kr needs to be kept small. For 10% Kr, the KrF^* formation efficiency by discharge pumping under stable and controlled conditions can be as high as 30-35%, as shown in Figure 7.

---

(27) C.H. Chen, J.P. Judish, and M.G. Payne, "Energy Transfer Processes in Ar-Xe and Ar-F_2 Mixtures," (unpublished).

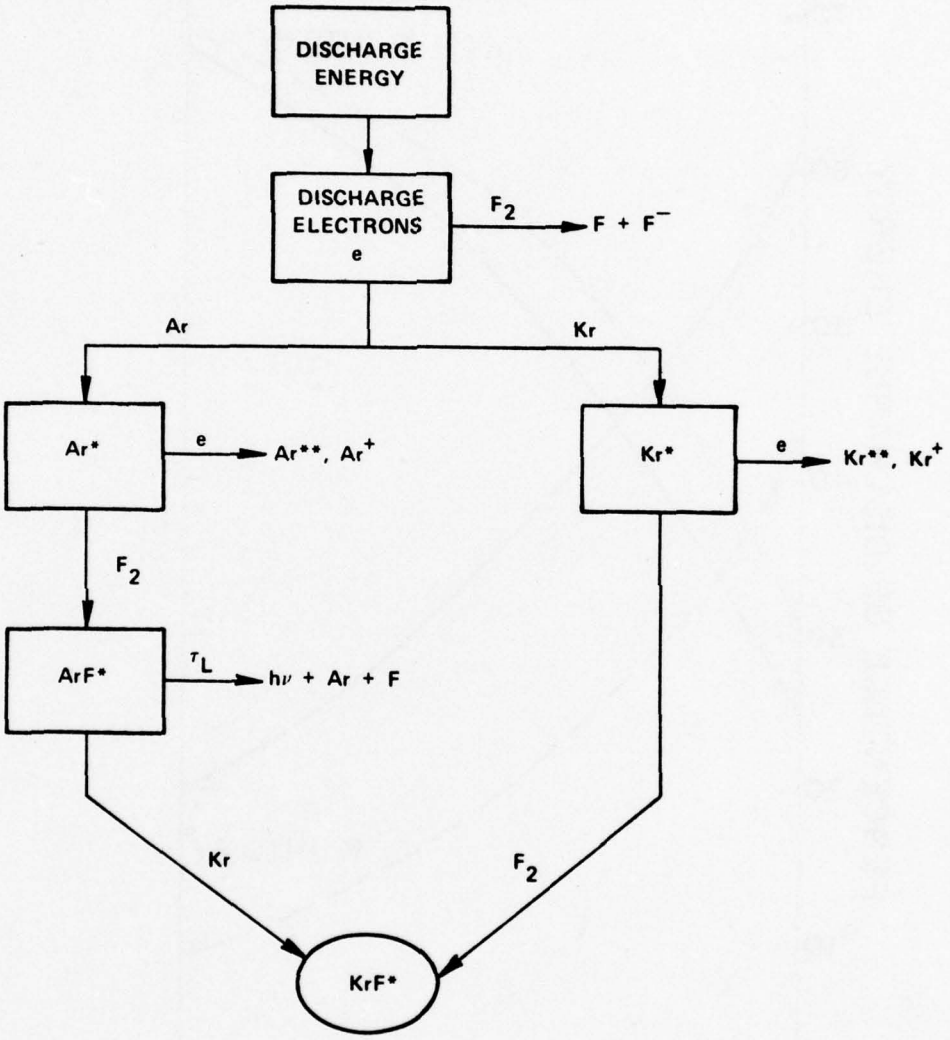

- DISCHARGE STABILITY: $\beta > 2\nu_{i0}$
- KrF* PRODUCTION EFFICIENCY ≃ 30–35%

G9333

Figure 5 Dominant Formation Kinetics of Discharge Pumped KrF*

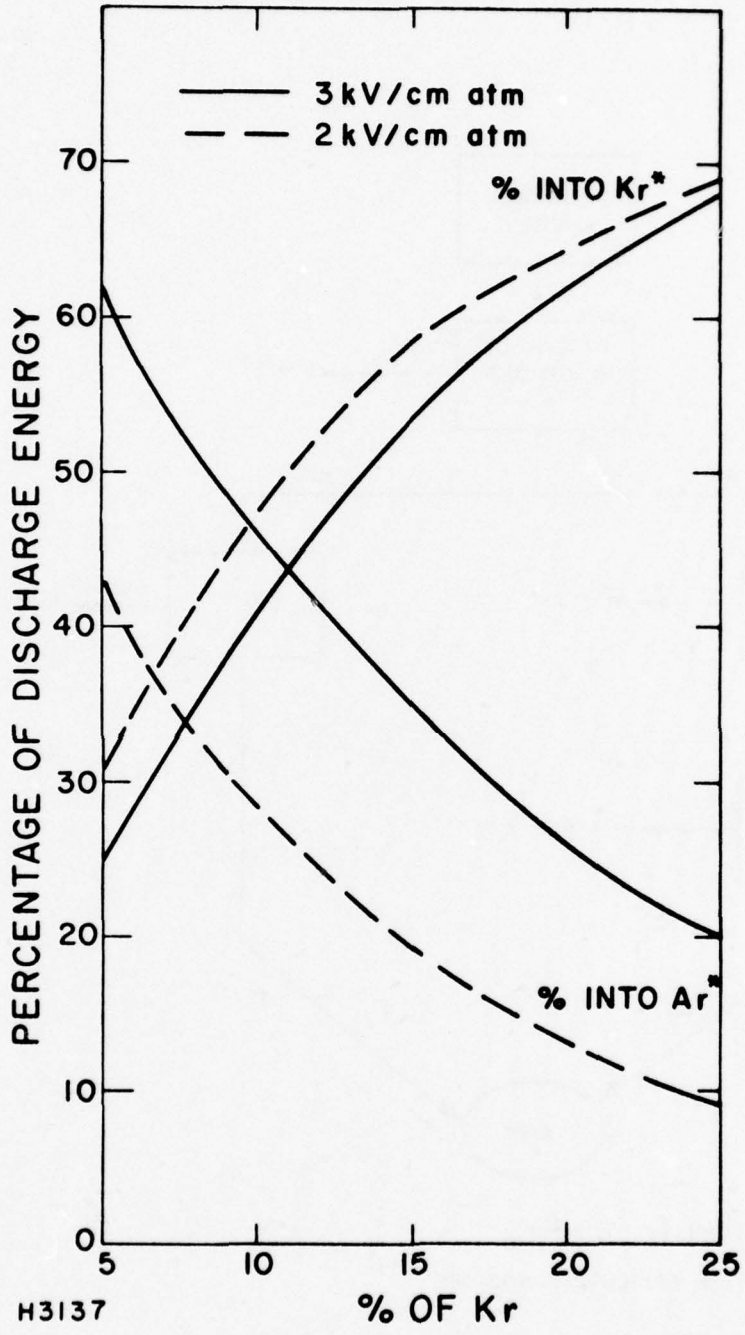

Figure 6 Percentage of Discharge Energy into Ar* and Kr* as a Function of Fractional Kr Density for Ar/Kr Mixtures

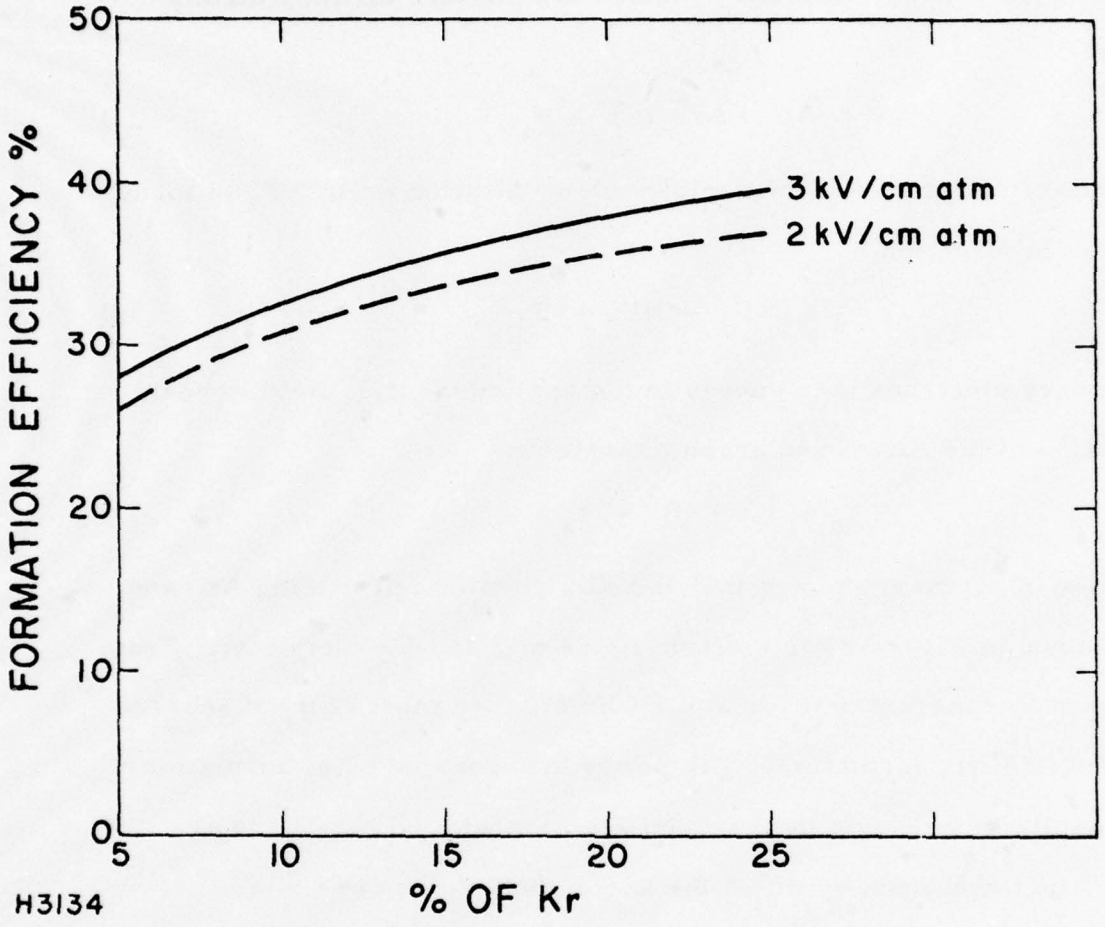

Figure 7 Formation Efficiency of KrF* as a Function of Fractional Kr Density

D. DISCHARGE PUMPED XeF^*

We will first discuss the formation kinetics in $Ar/Xe/NF_3$ mixtures.

The high energy electrons $\vec{e}$ ionize the mixture forming mainly argon ions

$$\vec{e} + Ar \rightarrow Ar^+ + \vec{e} + e_s \quad (1)$$

The secondary electrons e_s are rapidly lost by attachment to NF_3 to form the negative halogen ion

$$e_s + NF_3 \rightarrow NF_2 + F \quad (2)$$

The secondary electrons gain energy in the applied electric field to enable the excitation of the Xenon and argon metastables

$$e_s + R \rightarrow R^* + e_s \quad (3)$$

The fraction of discharge power that initially goes into producing Ar^* and Xe^* are shown in Figure 8 for electric fields of 2 and 3 kV/cm atm. From this figure it is apparent that for a 0.5% Xe mixture most of the discharge power goes into Ar^* formation. The power that goes into Xe^* formation rapidly results in XeF^* via the harpoon reaction with NF_3. There are three principal reactions by which the argon metastables are lost

$$Ar^* + Xe \rightarrow Xe^{**} + Ar \quad (4)$$

$$Ar^* + 2Ar \rightarrow Ar_2^* + Ar \quad (5)$$

$$Ar^* + NF_3 \rightarrow ArF^* + NF_2 \quad (6)$$

The rate constant for reaction (4) has been measured to be 1.8×10^{-10} and 3×10^{-10} cm^3/sec for Ar ($^3P_2$) and Ar ($^3P_0$) respectively.[28] Reaction (5) has a three-body rate constant of 1.7×10^{-32} cm^6/sec for Ar ($^3P_1$),

(28) L.G. Piper, J.E. Velazco and D.W. Setser, J. Chem, Phys. 59, 3323 (1973).

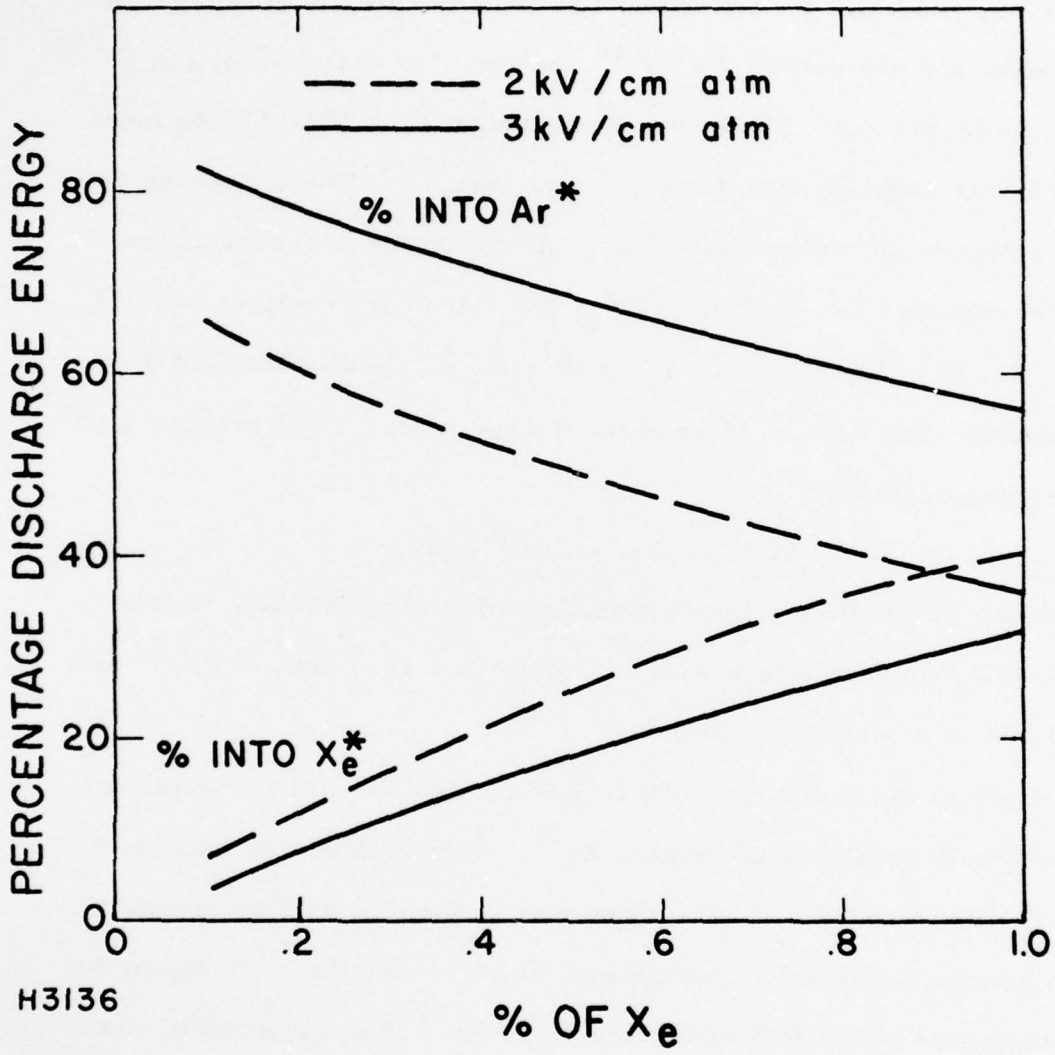

Figure 8 Percentage of Discharge Energy into Ar* and Xe* for Ar/Xe Mixtures as a Function of Fractional Xe Densities

0.9×10^{-32} cm^6/sec for Ar ($^1P_1$) and 1.6×10^{-32} cm^6/sec for Ar ($^3P_2$).[29] Assuming a gas kinetic mixing rate of these states by electrons, the loss rates of Ar^* by reactions (4) and (5) will be only marginally affected. So we will assume a mean rate of 2×10^{-10} cm^3/sec for reaction (4) and 10^{-32} cm^3/sec for reaction (5). The argon metastables react with NF_3 to form ArF^* with a rate constant of 1.4×10^{-10} cm^3/sec.[30] The branching ratio for this reaction is yet to be determined. At a mixture pressure of four atmospheres with 0.5% Xe and 0.1% NF_3, the rates for reactions (4), (5) and (6) are 8×10^7, 2.5×10^7 and 1.4×10^7 sec^{-1}. So about 15% of the Ar^* is channeled into ArF^*. Most of the energy in ArF^* will produce XeF^* by the following reaction

$$ArF^* + Xe \rightarrow XeF^* + Ar \qquad (7)$$

The remainder of the energy is presumably radiated on the ArF^* bands. As reaction (7) proceeds with a rate constant 1.6×10^{-9} cm^3/sec,[31] 80% of the ArF^* is to be channeled into XeF^*.

The argon excimers Ar_2^* will be deactivated at least as rapidly by Xe to form highly excited xenon states Xe^{**}. This means that 70-80% of the Ar_2^* will end up as Xe^{**}. The remainder of the Ar_2^* will be radiated. So we can conclude that the argon metastables transfer their energy to the xenon metastables with a 80% efficiency. The Xe^{**} thus formed will react with the NF_3 to form XeF^*. The branching ratio and rate constant for this

---

(29) M. Bourene, O. Dutnuit and J. LeCalve, J. Chem. Phys. 63, 1668 (1975).

(30) J.E. Velazco, J.H. Kolts and D.W. Setser, J. Chem. Phys. 65, 3468 (1976).

(31) M. Rokni, J.H. Jacob, J.A. Mangano and R. Brochu, "Formation and Quenching Kinetics of ArF," Appl. Phys. Lett. 31, 79-82, (1977).

reaction are not known. However, from discharge data it has been inferred a reaction rate constant of 4×10^{-10} cm^3/sec and a branching ratio of 0.7.[32]

When the Ar buffer is replaced by Ne most of the discharge energy will result in Xe^* formation as shown in Figure 9. The Xe^* formation as shown in Figure 9. The Xe^* will produce XeF^* via a harpoon reaction with NF_3.

(32) J.H. Jacob, M. Rokni and J.A. Mangano, Semi-Annual Technical Report for period March 1975 to September 1976.

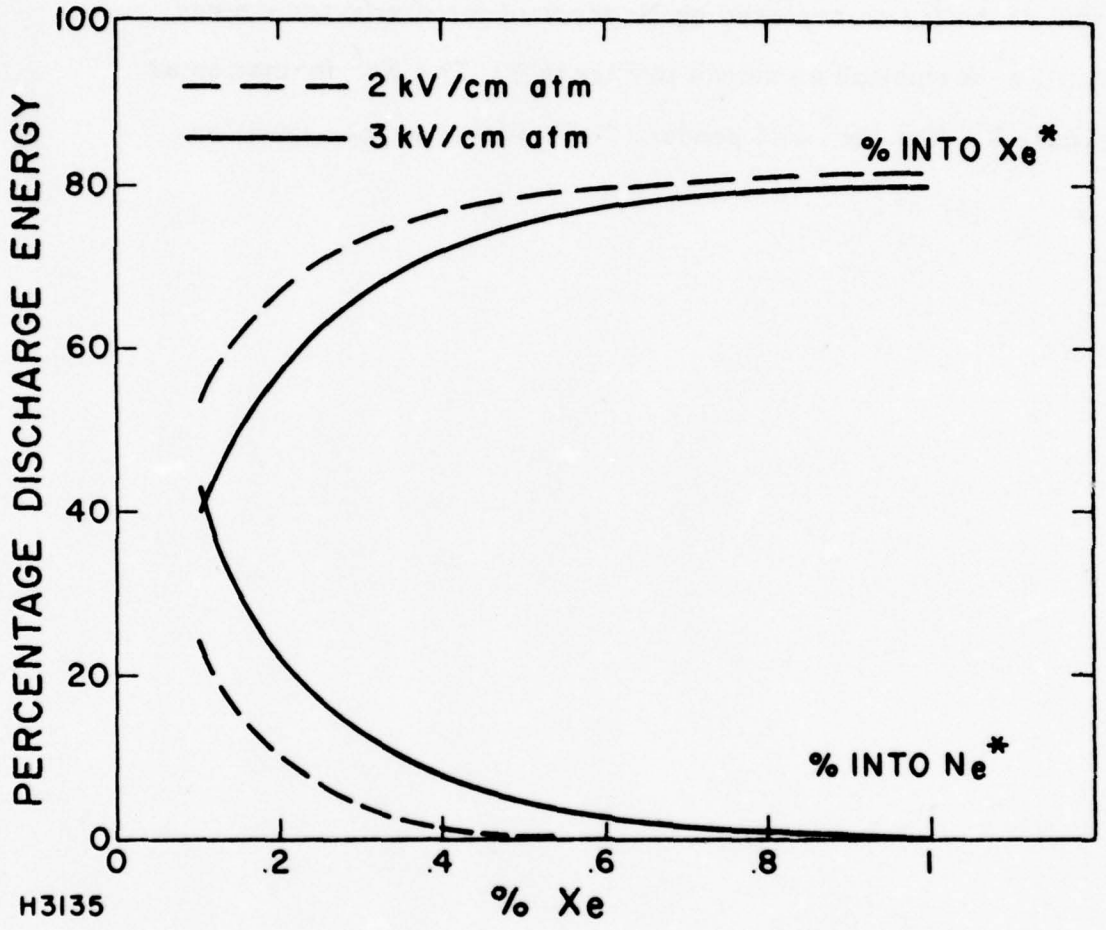

Figure 9 Percentage of Discharge Energy into Xe* and Ne* for Ne/Xe Mixtures as a Function of Fractional Xe Densities

III. QUENCHING KINETICS OF THE RARE GAS FLUORIDES

Once the excited rare gas fluoride is formed it can radiatively decay, be quenched by two and three body collisions with F_2, NF_3, and the rare gases, or under lasing conditions be stimulated by cavity flux. For efficient laser extraction the probability of stimulating the KrF^* should be much larger than the combined probability of decay by radiative and collisional processes. In the absence of a lower level the ratio of these probabilities is given by ϕ_c/ϕ_s, where ϕ_c is the cavity flux and ϕ_s is the saturation flux, which is defined by

$$\phi_s = \frac{h\nu}{\sigma_s}\left[\frac{1}{\tau_r} + K_x N_x + \sum_R K_R N_R + \sum_R K_{RR} N_R N\right] \qquad (8)$$

where $h\nu$ = photon energy; σ_s = stimulated cross-section; τ_r = the exciplex radiative lifetime; K_x is the two body quenching rate constant by the halogen donor; K_R and K_{RR} are the two and three body quenching rate constants by the rare gases. N_x and N_R are the number densities of the halogen donor, rare gas and N is the total number density.

A. DOMINANT QUENCHING PROCESSES OF KrF^*

The different measured quenching rate constants of KrF^* are listed in Table 2. These rate constants were determined by observing the KrF^* $B^2\Sigma_{1/2} \rightarrow X^2\Sigma_{1/2}$ radiation as a function of the partial pressures of the various gas constituents.[13, 33] It is of interest to note that the three body

---

(33) J.H. Jacob, M. Rokni, J.A. Mangano and R. Brochu, "Formation and Quenching Processes in Kr/F_2 Mixtures," to appear Appl. Phys. Lett. Jan. (1978).

TABLE 2. DOMINANT QUENCHING PROCESSES OF KrF*

Reaction		$k\tau_R(KrF^*)$	$k(\tau_R = 6.5\ nsec)$	
$KrF^* + F_2$	→ Products	$5 \times 10^{-18}\ cm^3$	$7.8 \times 10^{-10} cm^3 sec^{-1}$	(1)
$KrF^* + 2Kr$	→ $Kr_2F^* + Kr$	$4.4 \times 10^{-39} cm^6$	$6.7 \times 10^{-31} cm^6 sec^{-1}$	(2)
$KrF^* + Kr$	→ Products	$\leq 1.1 \times 10^{-20} cm^3$		(3)
$KrF^* + Kr + Ar$	→ $Kr_2F^* + Ar$	$4.2 \times 10^{-39} cm^6$	$6.5 \times 10^{-31} cm^6 sec^{-1}$	(4)
$KrF^* + 2Ar$	→ Products	$4.6 \times 10^{-40} cm^6$	$7 \times 10^{-32} cm^6 sec^{-1}$	(5)

quenching of KrF^* by Ar and Kr leads to the eventual formation of Kr_2F^* by the following reactions:

$$KrF^* + 2Ar \rightarrow Ar\,KrF^* + Ar \quad (9)$$

$$Kr + Ar\,KrF^* \rightarrow Kr_2F^* + Ar \quad (10)$$

$$KrF^* + Kr + M \rightarrow Kr_2F^* + M \quad (11)$$

The appearance of Kr_2F^* at high pressures is demonstrated in Figure 10. In this figure the spontaneous emission spectra from e-beam excited mixtures were obtained at mixture pressures of 0.5, 2 and 4 atm. The uncalibrated intensity scale is approximately logarithmic. At 0.5 atm essentially all of the radiation from the mixture is contained in the KrF^* $B^2\Sigma_{1/2} \rightarrow X^2\Sigma_{1/2}$ band of 248 nm. However, two other broadbands, containing much less energy, are observable. The first is the Kr_2F^* ($^2B_2 \rightarrow A_1$) centered at 415 nm. The other broadband, centered roughly at 270-280 nm, is most likely a combination of radiation from the $^2\Sigma \rightarrow {}^2\Pi$ of KrF^* and perhaps radiation from the excited triatomics Ar_2F^* and $Ar\,KrF^*$. The spectrum obtained at a total mixture pressure of 4 atm indicates that, compared with the 0.5 atm spectrum, essentially the same energy is contained in the KrF^* $B^2\Sigma_{1/2} \rightarrow X^2\Sigma_{1/2}$ band, although the energy deposited increased by a factor of ≈ 8. This spectrum indicates that most of the additional energy deposited by the e-beam was channeled into Kr_2F^*, by the quenching processes discussed above.

B. DOMINANT QUENCHING PROCESSES OF XeF^*

The two and three body quenching rate constants of XeF^* by F_2, NF_3 and the rare gases are listed in Table 3. From this table it is clear that the quenching of XeF^* by Ne is significantly slower than by Ar. This

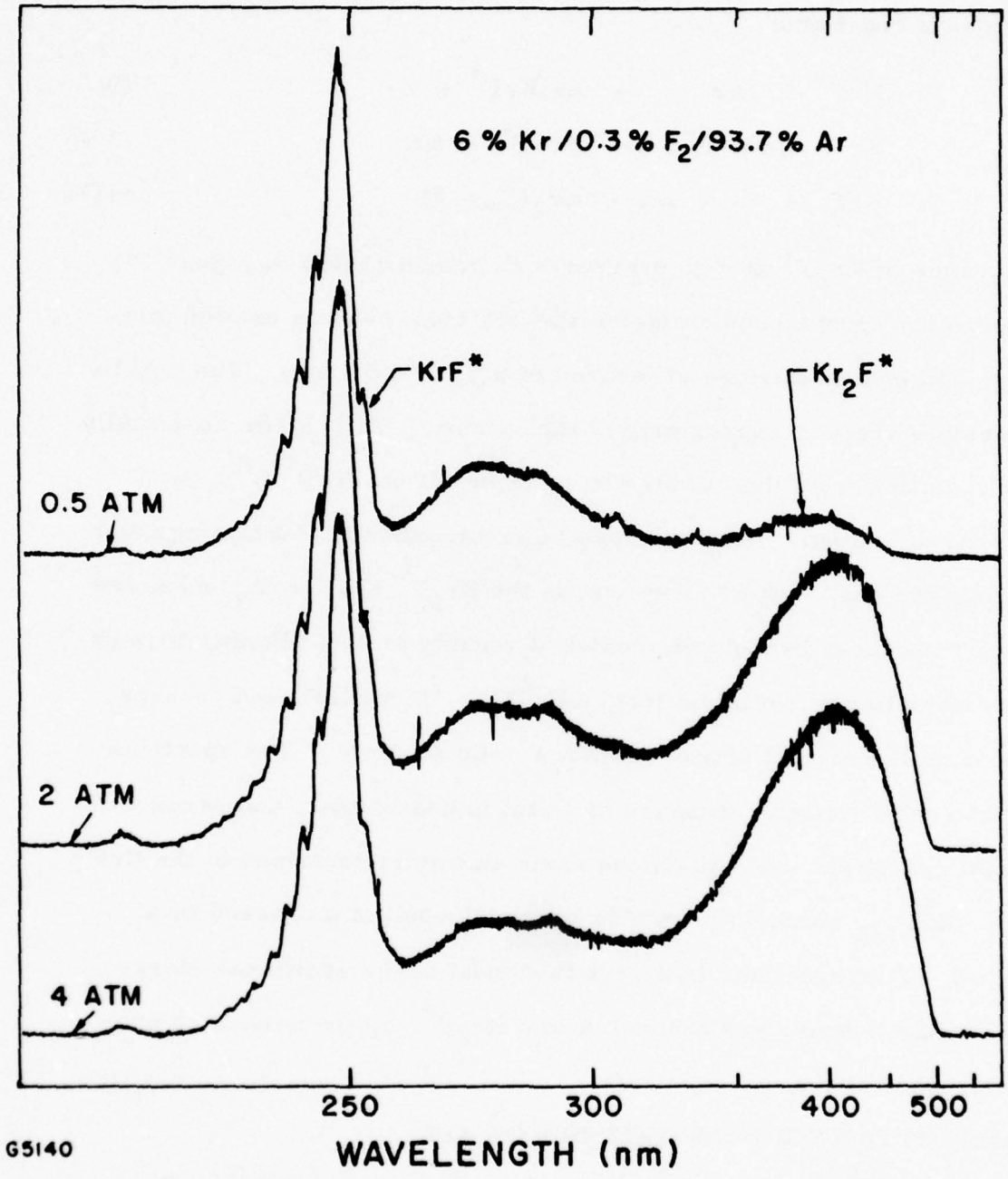

Figure 10 Spectra from a KrF* Laser Mix at Various Total Pressures

TABLE 3. DOMINANT XeF^* QUENCHING PROCESSES

Reaction	$k\tau_r$	$k(\tau_r = 16\ ns)$
$XeF^* + F_2$	$5.3 \times 10^{-18} cm^3$	$3 \times 10^{-10} cm^3/sec$
$XeF^* + NF_3$	$2.8 \times 10^{-19} cm^3$	$1.7 \times 10^{-11} cm^3/sec$
$XeF^* + Xe$	$4.5 \times 10^{-19} cm^3$	$2.9 \times 10^{-11} cm^3/sec$
$XeF^* + Ne$	Negligible	
$XeF^* + Xe + Ne$	$1.23 \times 10^{-38} cm^6$	$7.7 \times 10^{-31} cm^6/sec$
$XeF^* + 2Ne$	$4.32 \times 10^{-41} cm^6$	$2.7 \times 10^{-33} cm^6/sec$
$XeF^* + Ar$	$1.28 \times 10^{-20} cm^3$	$8 \times 10^{-13} cm^3/sec$
$XeF^* + 2Ar$	$2.4 \times 10^{-40} cm^6$	$1.5 \times 10^{-32} cm^6/sec$
$XeF^* + Xe + Ar$	$4.8 \times 10^{-39} cm^6$	$3 \times 10^{-31} cm^6/sec$

is one of the reasons that Ne is a better diluent than Ar in the XeF^* laser. One main difference between the quenching processes of XeF^* and KrF^* is that two-body quenching by the rare gases plays a more important role in XeF^* than in KrF^*. This is especially true of the quenching of XeF^* by Xe as compared to the quenching of KrF^* by Kr.

IV. PUMPING CONSIDERATIONS

As we have mentioned in the Introduction, the three main pumping methods are: (a) pure e-beam pumping; (b) e-beam controlled discharge pumping; and (c) UV preionized (avalanche) discharge pumping. In this section we will discuss these pumping methods and their peculiar problems.

A. E-BEAM PUMPING

The use of high energy electrons has greatly advanced the technology of high power lasers. Fast electrons were first used as a source of ionization in high pressure CO_2 lasers.[34] They were subsequently used for the direct pumping of the rare gas excimer[35] and rare gas monohalide lasers.[3,5] In fact, all the excimer and exciplex lasers were first pumped by high energy e-beams. More recently they have been used as a partial source of ionization in discharge pumping of the KrF^* and XeF^* lasers.[9] One of the scaling limitations of these lasers is the magnetic field resulting from the discharge current and self magnetic field of the beam that causes the beam to pinch. Boyer, Henderson and Morse[36] have demonstrated the effects of the discharge magnetic field on the fast electrons by Monte Carlo

---

(34) J. D. Daugherty, E. R. Pugh, and D. H. Douglas-Hamilton, Bull. Am. Phys. Soc. 16, 399 (1971); C. A. Fernsternmacher, M. J. Nutter, J. P. Rink and K. Boyer, Bull Am. Phys. Soc. 16, 42 (1971).

(35) H. A. Koehler, L. J. Ferderber, D. L. Redhead and D. J. Ebert, Appl. Phys. Lett. 21, 198 (1972); P. W. Hoff, J. C. Swingle and C. K. Rhodes, Appl. Phys. Lett. 23, 245 (1973).

(36) K. Boyer, D. B. Henderson and R. L. Morse, J. Appl. Phys. 44, 5511 (1973).

simulations. These authors have also shown that a guide magnetic field can reduce and eliminate the effects of pinching. Mangano[37] has recently shown the effects of e-beam pinching resulting from a self magnetic field. He has also demonstrated that a guide magnetic field eliminates this effect. In fact, with the application of a guide magnetic field, the performance of a direct pumped KrF^* output energy increased by a factor of four.[10] The increased laser performance is a direct result of more efficient coupling of the e-beam into the laser mixture.

Electron beams are widely used because of their availability, and ability to deposit relatively large power densities uniformly and large volumes in the laser mixture. The pump power P required to obtain lasing action for a repulsive lower level is given by

$$P \gtrsim \frac{gE}{\eta \tau \sigma_s L} \tag{12}$$

where g is the required single pass gain, τ the exciplex lifetime, σ_s the stimulated cross section, L the length of the active medium, E the energy of the upper level and η the efficiency of exciting the upper level. So for a gain of 20%, a lifetime of 10 nsec, efficiency of 10%, length of 20 cm, $\sigma_s = 10^{-16}$ cm^2 and $E \approx 5$ eV.

$$P \gtrsim 10^5 \text{ W/cm}^3 \tag{13}$$

Such high pump powers are easily obtained by e-beams.

In this section we discuss electron scattering in gases by assuming that the fast electrons can be described by a current and number density. Such a simplification is not valid for a well collimated beam. However,

---

(37) J.A. Mangano, AERL (unpublished).

the high energy electrons have first to pass through a foil; if the foil thickness is greater than 2/5 of the transport mean free path, then the fast electrons, after traversing the foil, are fairly diffuse.[38, 39] Further, by a superimposition of two isotropic sources, a well collimated beam may be treated by the diffusion theory. For a diffuse beam, in the absence of an electric and magnetic field, one can use the "age" theory.[38] In addition, the age theory has been extended to include the effects of the discharge electric field.[40] The importance of the electric field can be assessed by considering the dimensionless parameter γ, which is the energy gained per transport mean free path divided by the electron energy. Typically, in an e-beam controlled discharge $\gamma \approx 0.1 - 0.3$ and the effect of the electric field on fast electrons is small, so we will ignore it.

Besides the effect of imposed electric fields it is necessary to consider the effect of both self magnetic fields and imposed magnetic fields. Diffusion in the presence of a magnetic field can generally be separated into two directions: diffusion along and perpendicular to the field direction. This analysis is similar to diffusion of a plasma in a magnetic field. The diffusion across the magnetic field is restricted because the electrons will tend to gyrate around the magnetic field. In fact, the diffusion across the field lines will be reduced by a factor $(1 + \lambda^2/r_\ell^2)^{-1}$ where λ is the transport mean free path and r_ℓ is the Larmor radius.[41] However, because of the

---

(38) H. A. Bethe, M. E. Rose, L. P. Smith, Proc. Am. Philos. Soc. 89, 1256 (1938).

(39) J. H. Jacob, J. Appl. Phys. 45, 467 (1974).

(40) H. A. Bethe and J. H. Jacob, "Diffusion of Fast Electrons in the Presence of an Electric Field," Phys. Rev. A16, 1952 (1977).

(41) J. H. Jacob, "Diffusion of Fast Electrons in the Presence of a Magnetic Field," Appl. Phys. Lett. 31, 252-254 (1977).

energy dependence of λ and r_ℓ the resulting diffusion perpendicular to the magnetic field is a complicated function of magnetic field strength B and the electron energy. In the limit of large B the diffusion perpendicular to field lines turns out to be inversely proportional to the magnetic field strength.[41] Reasonable magnetic field strengths can in fact be imposed to good advantage. For typical rare gas laser mixtures and pressures λ/r_ℓ is $\gg 1$ for magnetic fields of 1 kG.

In the presence of a strong magnetic field, only the diffusion of electrons in the direction of the field need be considered. The half space solution for this case simplifies to[40]

$$N_h(x, t) = N(x - 0.4\lambda, t) - N(x - 1.82\lambda, t) \tag{14}$$
$$= \frac{1}{\chi}\sqrt{t}\left[\exp - \frac{(x - 0.4\lambda)^2}{4t} - \exp - \frac{(x + 1.82\lambda)^2}{4t}\right]$$

where N_h = energy deposition, x = distance along the beam, and t = electron age. To obtain the energy deposition one has to integrate overall t. Figure 11 shows the solution for a mixture containing 95.7% Ar and 4% Kr and 0.3% F_2 at a total pressure of 1.7 atm. In this calculation we have also allowed for a 2 mil Kapton foil.

The most efficient way to couple e-beam energy into the laser mixture is by using two e-beams. The resulting energy deposition from such a configuration is shown in Figure 12. Using two e-beams together with a magnetic field 90% of the fast electron energy can be coupled into the laser mixture with a variation in the energy deposition of $\pm$ 10%.

B. DISCHARGE PUMPING

The two discharge pumping methods are e-beam controlled discharge pumping and UV preionized avalanche discharge pumping. By e-beam

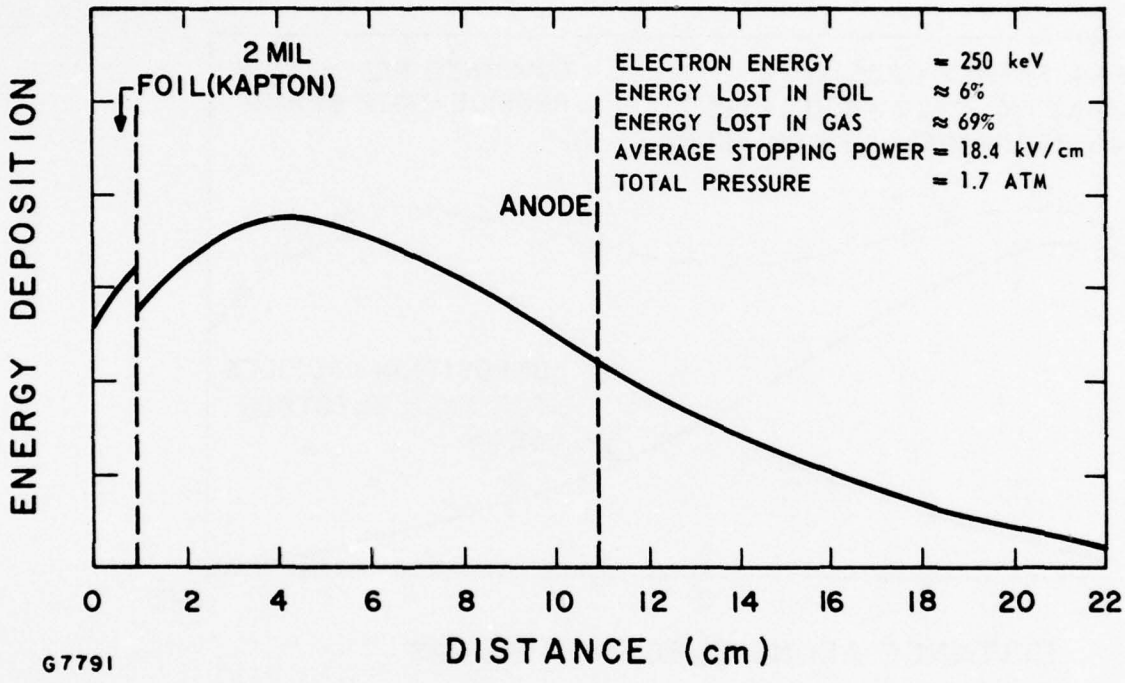

Figure 11 E-Beam Energy Deposition in a $Ar/Kr/F_2$ Mixture at Total Pressure of 1.7 atm

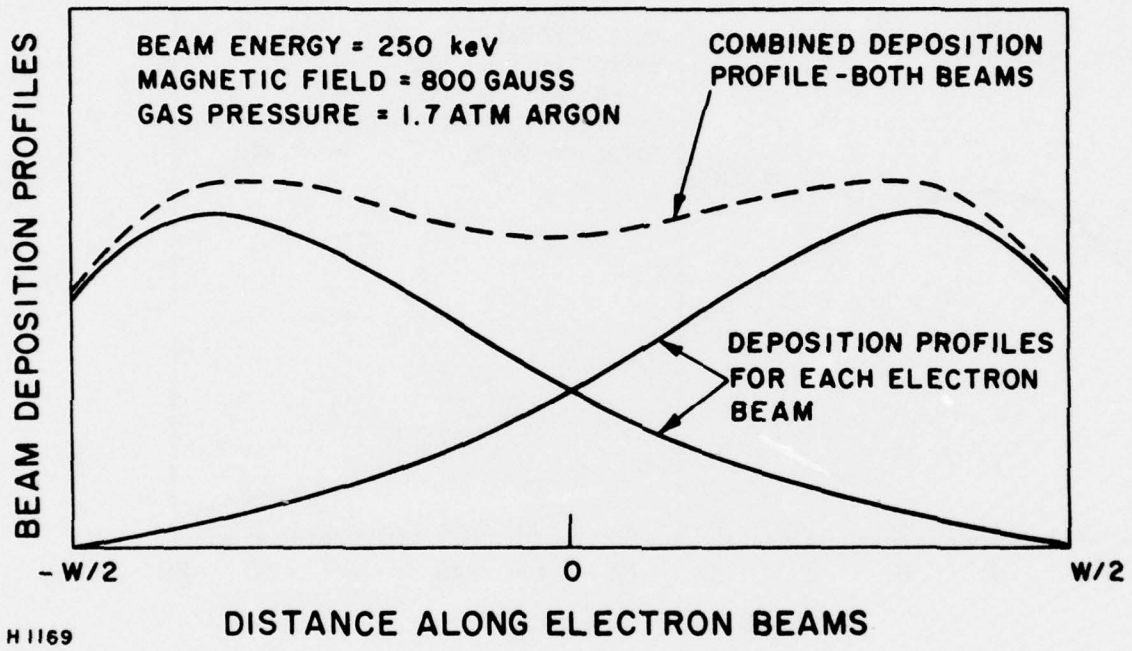

Figure 12 Predicted E-Beam Deposition When Two E-Beams are Used

controlled discharge pumping most, but not all, the discharge electrons are produced by a high energy e-beam. The discharge, which provides most of the pump power is then run in the ionization produced by the fast electrons. In UV preionized discharge pumping the laser medium is preionized by UV radiation.

1. Metastable Production Efficiency

The discharge physics is strongly affected by electron impact excitation and ionization of the rare gas metastables. To model these effects we have treated the krypton metastable as rubidium and the argon metastable as potassium. This analogy has been used successfully in predicting the emission spectra of the excited rare gas monohalides and is justified physically by the atomic similarity between rare gas metastables and the alkalis.[23] Some of the electron impact cross sections used in our model are shown in Figure 13. The cross section for excitation from the 5 s configuration to the 5p configuration in Rb[42] (Kr^*) has a peak value of 75 $Å^2$ at 8 eV. Also shown are the ionization cross section of Rb[43] (Kr^*) and the excitation[44] and ionization[45] cross sections of ground state Ar. From Figure 13 it is clear that the peak value of the metastable Ar excitation cross section is 30 times the peak value of the excitation cross section of Ar from the ground state. More important, however, is the fact that most of the electrons can excite the 5s to 5p transitions which have a threshold of 1.6 eV, resulting

(42) H. Hyman, AERL private communication.

(43) R. H. McFarland and J. D. Kinney, Phys. Rev. 137, 1058 (1965).

(44) J. H. Jacob and J. A. Mangano, "Total Electron Impact Excitation Cross Sections of Ar and Kr," Appl. Phys. Lett. 29, 267-469 (1976).

(45) D. Rapp and P. Englander-Golden, J. Chem. Phys. 43, 1464 (1965).

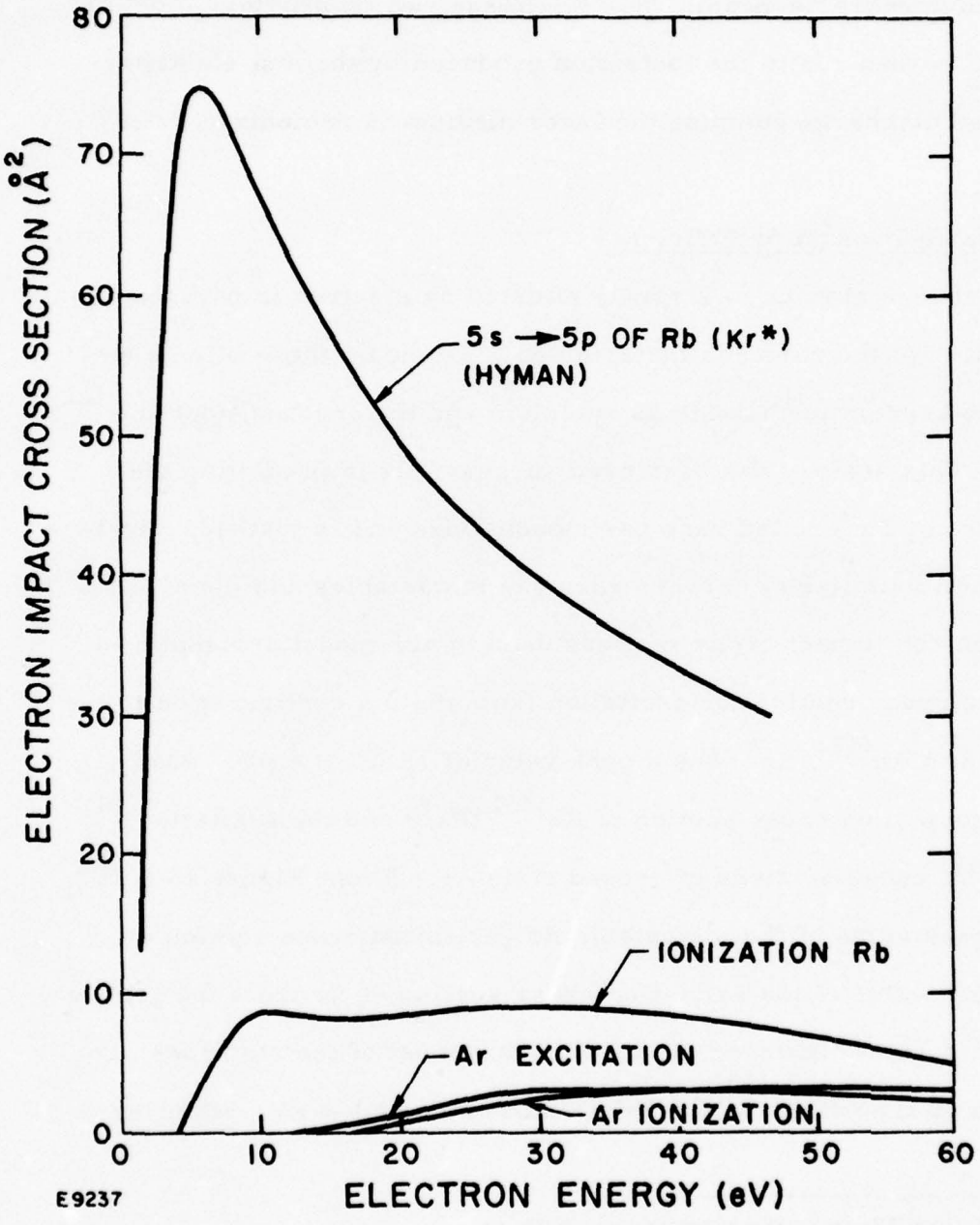

Figure 13 Electron Impact Cross-Section for Rb (Kr*) and Ar as a Function of Electron Energy

in a cooling of the electrons whereas only the high energy tail of the electron energy distribution can produce metastables from the ground state. We have put these cross sections into a computer code which solves the Boltzmann electron transport equation. This Boltzmann code takes the cross section data and the electric field and calculates self-consistently the electron energy distribution and the partitioning of discharge energy amongst the various excited states and ionization. The predictions of the code are shown in Figures 14, 15, 16.[46] Figure 14 shows the percentage of energy that goes into producing Kr^* as a function of the fractional metastable population $Kr^*/(Kr + Ar)$ for electric fields of 2-6 kV/cm atm. It is apparent from Figure 14 that the efficiency of producing the metastables is a strong function of the Kr^* population. For example, the efficiency of forming Kr^* is almost 60% when the fractional population is 10^{-5} and the electric field is 2 kV/cm atm. This efficiency decreases to less than 10% when the fractional population is increased to 10^{-4}. The decrease in efficiency is because the increased Kr^* density cools the electrons. Figure 15 is a plot of the average electron energy as a function of the fractional metastable population increases. The cooling effect is much stronger at smaller electric fields. The decrease in efficiency can be made up by increasing the electric field. However, the ionization rate (see Figure 16) rapidly becomes so large that it precludes discharge stabilization by electron attachment (F_2) (see

(46) Recent calculations by W. H. Long, Jr., "Electron Kinetics in the KrF Laser," Appl. Phys. Lett. 31, p. 391-394 (1977) have shown that electron - electron collisions will effect the discharge kinetics for a reduced electric field of $< 10^{-16}$ V-cm^2 and fractional electron densities of $>10^{-5}$. Similar calculations have also been performed by William H. Nyhan of United Technologies. The discharge data presented in the following sections are for electric fields $>10^{-16}$ V-cm^2 and maximum fractional electron densities $\leq 2 \times 10^{-5}$. For these conditions electron-electron collisions will have a 10% effect on the discharge kinetics.

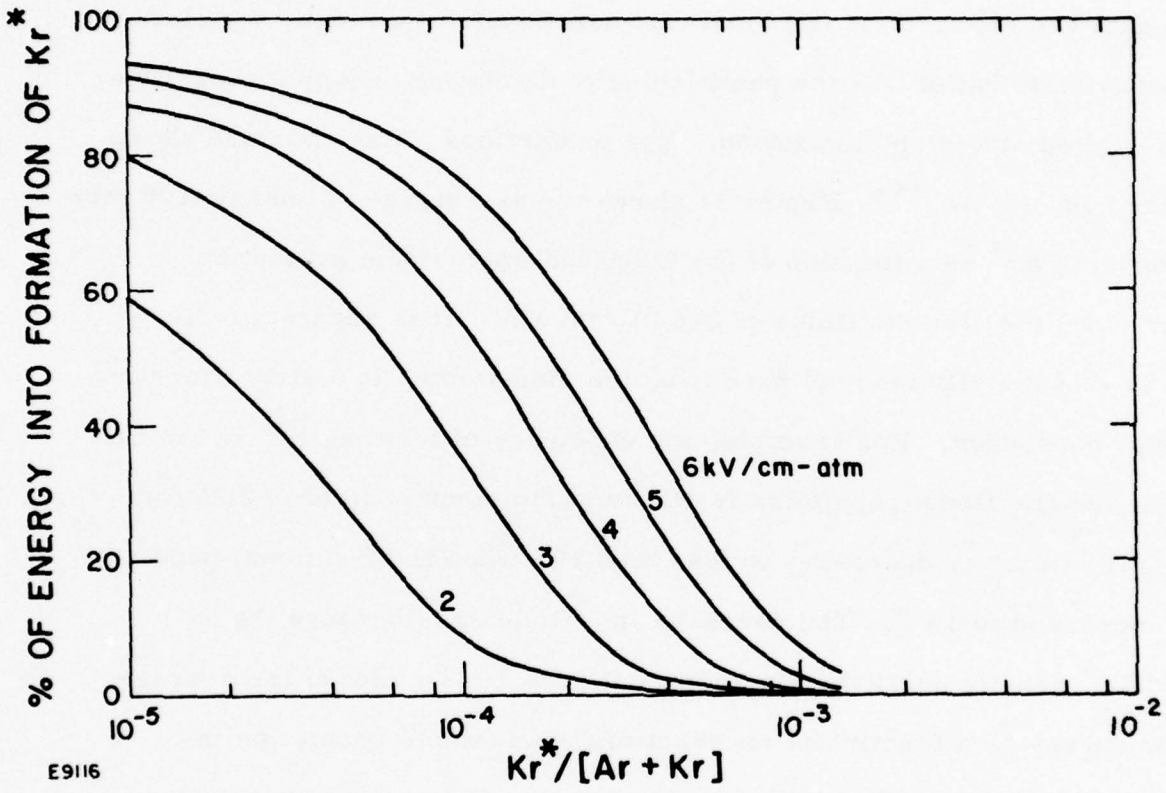

Figure 14 Percentage of Discharge Power into Kr* as a Function of Fractional Kr* Population for Various Applied

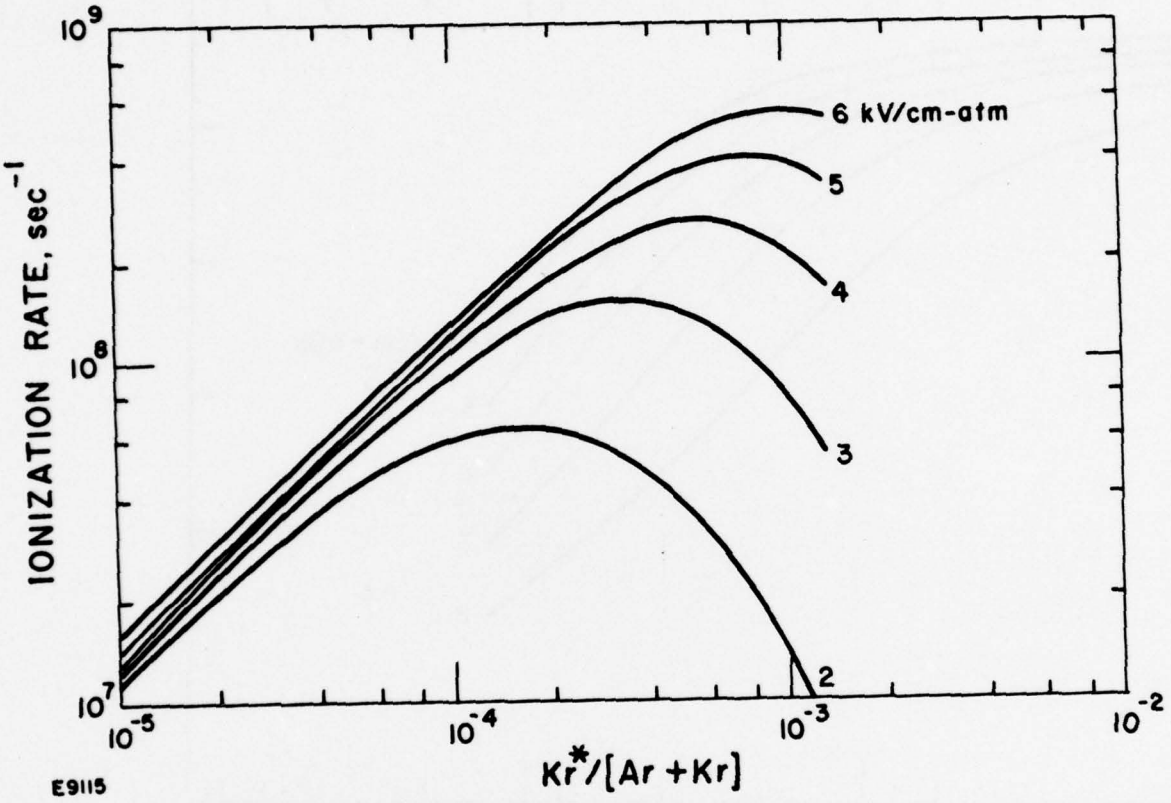

Figure 15 Ionization Rate as a Function of Fractional Kr* Population

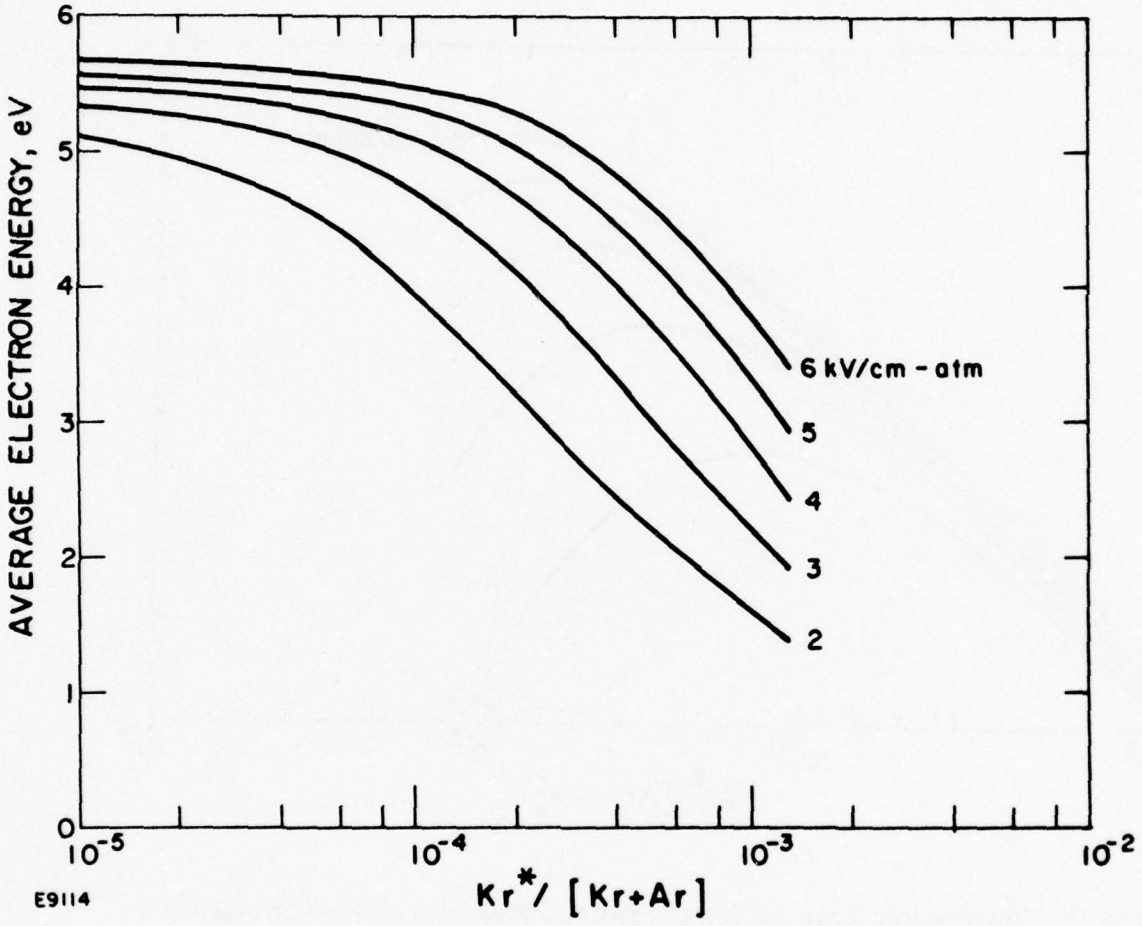

Figure 16 Average Electron Energy as a Function of Fractional Kr* Population

following section) for cases where the discharge power exceeds the e-beam power into the laser medium.

Under controlled discharge conditions one can choose the desired operating conditions and insure that the fractional metastable population is small enough so that the metastable production efficiency is high. In the case of the UV preionized discharge, however, the current and hence the power density and fractional metastable population increases in an uncontrolled manner. As a result, the metastable production efficiency will decrease and will be smallest when the power into the laser mixture is the largest. This is one of the reasons that the UV preionized discharges can only achieve efficiencies of 1%. Another reason, as we will discuss subsequently, is that the increased power density results in an increased excited state density and a relatively large absorption at the laser frequency. Hence the optical extraction efficiency is adversely affected.

2. Discharge Stability

The discharge stability of these mixtures is strongly affected by the rare gas excited states. This becomes clear from the following simple analysis. Typically the input energy for efficient laser action is 100 J/liter-μsec. So the discharge power that goes into producing metastables directly is given by

$$P_m = \eta_m \times 10^5 \text{ kW/cm}^3 \qquad (15)$$

The metastable lifetime is determined primarily by the halogen donor like F_2. In the presence of 0.2% F_2 at a mixture pressure of 2 atm, the rare gas metastable lifetime τ_o is about 15 ns. Assuming that η_m = 50% the steady state metastable density M^* is about 5×10^{14} cm^{-3} and the fractional population is 10^{-5}. For these conditions the electron impact ionization of the

mestastable is 2×10^7 sec^{-1} compared to 10^3 sec^{-1} for the ground state. Hence, metastable ionization is the dominant ionization for laser discharge conditions. The production and loss of discharge electrons n_e is given by

$$\frac{dn_e}{dt} = S + (\nu_i - \beta) n_e \tag{16}$$

where S is the electron/ion production rate, ν_i is the ionization frequency and β, the attachment rate.

The production and loss of the metastables is

$$\frac{dM^*}{dt} = \langle \sigma v \rangle n_e M - \frac{M^*}{\tau_d} \tag{17}$$

As we have discussed above, the dominant ionization is metastable ionization, so we can write

$$\nu_i = \langle \sigma v \rangle_i M^* \tag{18}$$

Equations (16) and (17) are a pair of nonlinear coupled differential equations in n_e and ν_i. By a perturbation analysis it can be shown[47] that these equations predict a nonzero steady state solution for n_e if

$$S \neq 0 \quad \beta \geq 2\nu_{i0} \tag{19}$$

where ν_{i0} is the equilibrium ionization rate. From the stability criterion it is clear that UV preionized discharges will not be stable because the electron production occurs prior to the discharge pulse.

The electrons freed by photoionization rapidly form negative halogen ions

$$e + X_2 \rightarrow X^- + X \tag{20}$$

---

(47) J. D. Daugherty, J. A. Mangano, and J. H. Jacob, "Attachment-Dominated Electron-Beam Ionized Discharges," Appl. Phys. Lett. 28, 581-582 (1976).

The negative ions then provide and easily ionizable source for production of discharge electrons.[48] Electron detachment presumably occurs by discharge-electron impact and laser-photon detachment. The negative ions which are lost by recombination result in a more uniform spatial distribution. When the discharge electric field is applied the electron density avalanches rapidly by several orders of magnitude, and large discharge-energy inputs are possible. The key issues to be addressed in e-beam sustained discharge pumping are discharge stability and discharge enhancement.

We have numerically solved a system of nonlinear equations similar to Eqs. (16) and (17) for e-beam current of about 2 A/cm^2. In this analysis we have also included Penning ionization and ionization of the ground state atoms. Figure 17 shows the results of such an analysis. On the left-hand side we have the stable discharge condition, i.e., the attachment rate is slightly greater than twice the equilibrium ionization rate. Notice that the discharge current reaches a constant value asymptotically. Another important feature for the stable discharge case is that the metastable production efficiency η_M remains above 75%. If we keep everything constant but decrease the attachment rate by 20% we observe that the ionization rate increases and after about 70 ns becomes greater than the attachment rate. For this case the discharge current increases faster than exponentially in time and the metastable production efficiency falls steeply. In Figure 18 we see experimental current, voltage and fluorescence traces for a KrF e-beam controlled discharge under stable and unstable operating conditions. The discharge cavity was filled to 2 atm with 0.1% F_2, 2% Kr and 97.9% Ar. Stable

(48) J.C. Hsia, "A Model for Preionization in Electric-Discharged-Pumped Xef and 1.1 Lasers," Appl. Phys. Lett. 30, pp. 101-103 (1977).

discharge conditions were achieved when the 0.3 μF capacitor was charged to 8 kV. Notice that the discharge current reaches a steady state value before the end of the e-beam current pulse. When the capacitor was charged to 10 kV the discharge was unstable. The discharge current increases slowly at first and has a shape very similar to the unstable case shown in Figure 17. The discharge current is volumetrically unstable before it arcs. This assertion is verified if one observes in Figure 18, that the fluorescence is increasing for 40 ns subsequent to the onset of rapid current growth.

3. Discharge Enhancement

In an e-beam controlled discharge one is interested in both discharge stability and large (≥ 5) discharge enhancement. The discharge enhancement is defined here as the ratio between the power deposited in the laser mix by the discharge P_d to the power deposited by the e-beam P_{eb}. This ratio is given by

$$\frac{P_d}{P_{eb}} = \frac{eV_D E}{(\beta - \nu_{i0})E_i} \tag{21}$$

where V_D is the average discharge electron drift velocity; E is the applied electric field and E_i is the energy required to create an electron-ion pair by the beam electrons. For discharge stability we have shown that $\beta \geq 2\nu_{i0}$, so for an e-beam stabilized discharge Eq. (21) can be rewritten as

$$\frac{P_d}{P_{eb}} \leq \frac{eV_D E}{\nu_{i0} E_i} \tag{22}$$

Using the curves in Figures 15 and 16, the ionization rate can be expressed as a function of the metastable production efficiency η_M for a given electric field. Thus we can plot the discharge enhancement factor as a function of the metastable production efficiency. Figure 19 shows such a plot for an

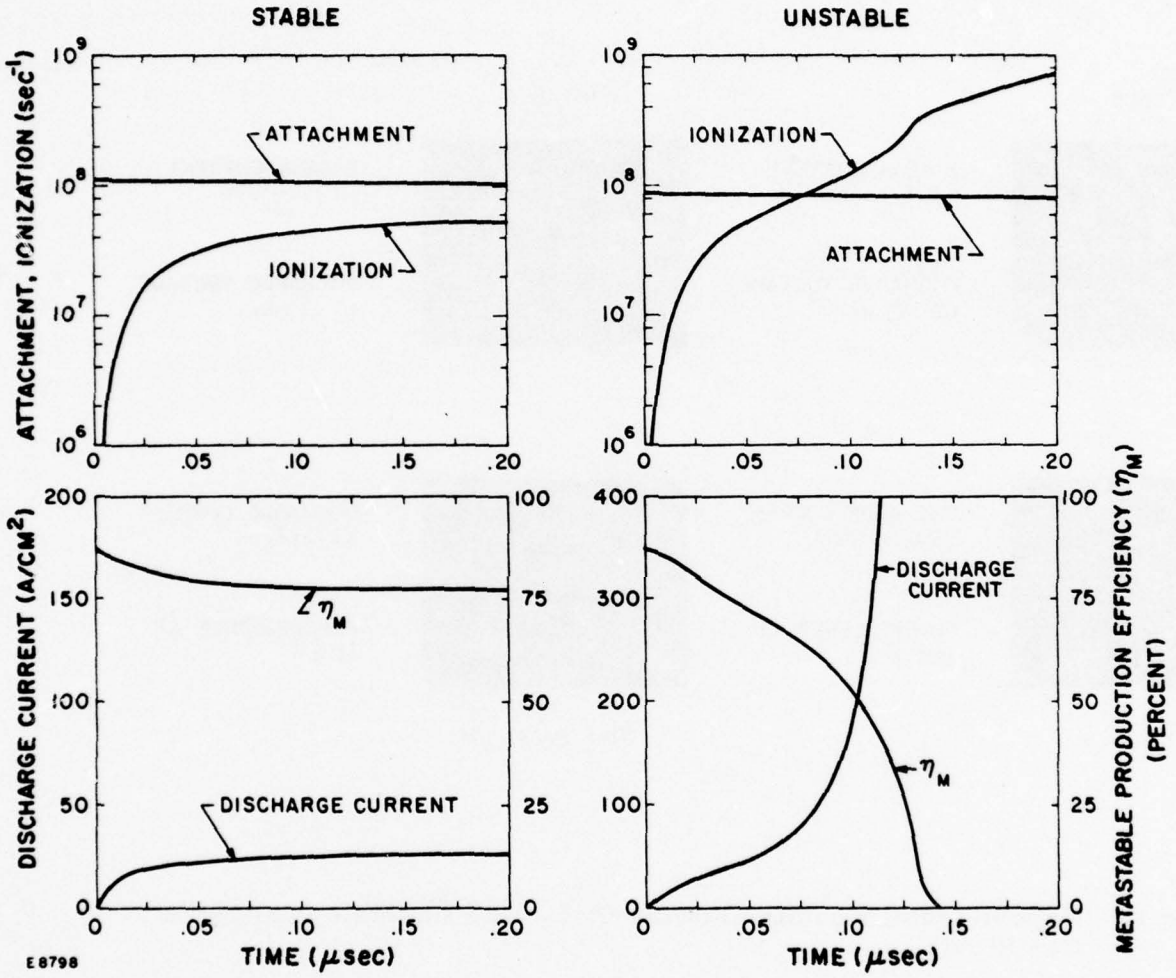

Figure 17 Results of a Numerical Analysis to a System of Equations Similar to Eqs. (16) and (17)

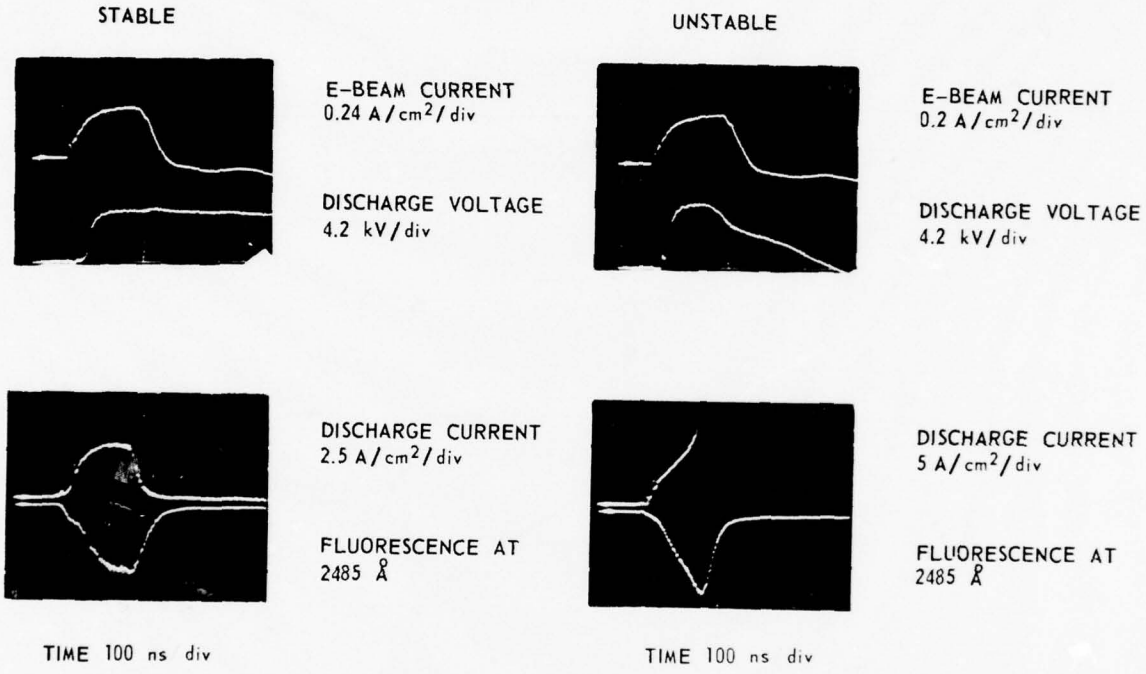

Figure 18 Experimental Results Showing Stable and Unstable Discharge Conditions

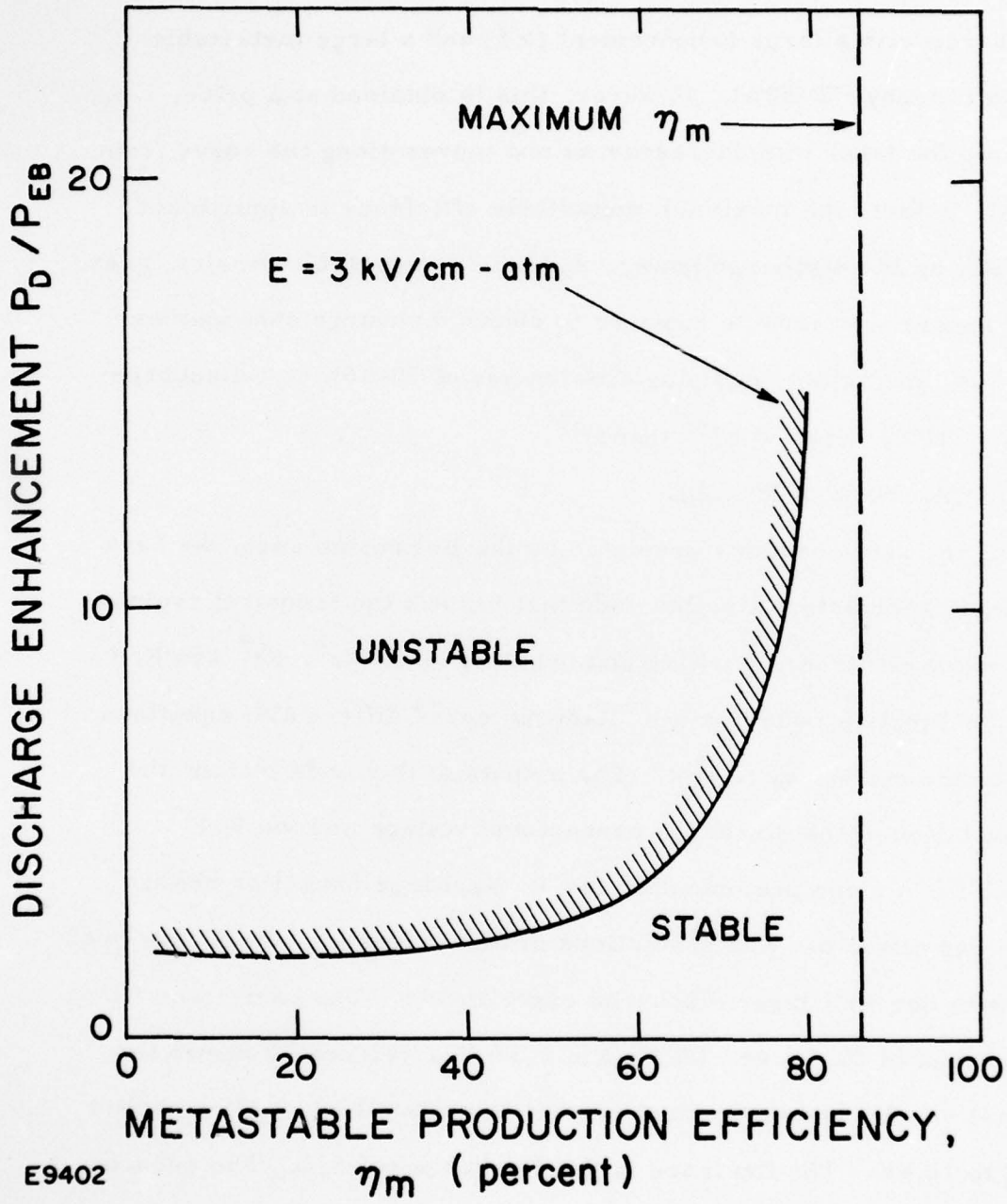

Figure 19 Plot of Discharge Enhancement as a Function of Metastable Production Efficiency for the Limiting Case of a Stable Discharge

electric filed of 3 kV/cm atm. The analysis predicts that one can obtain a stable discharge with a large enhancement (> 5) and a large metastable production efficiency (70-80%). However, this is obtained at a price, i.e., the power into the laser mix decreases as one moves along the curve from left to right. In fact, the maximum metastable efficiency is approached asymptotically as the discharge power, and hence metastable density, goes to zero. It appears reasonable however to obtain discharge enhancement factors of 5-10, metastable pumping efficiencies of 70-80% at a discharge power input of 100 J $(\text{liter-atm})^{-1}$ $(\mu\text{sec})^{-1}$.

C. KINETIC DISCHARGE MODEL

Using the rate constants predicted by the Boltzmann code, we have developed a self-consistent kinetics code that follows the temporal evolution of the secondary electrons, positive and negative ions, Ar^*, Kr^* and KrF^*. We couple our kinetics code to a simultaneous set of differential equations that describe the electrical circuit. The outputs of this code include the temporal evolution of the discharge current and voltage and the KrF^* fluorescence for a given preionization level, discharge capacitor charge voltage and gas mixture. The predictions of this discharge model have been compared with our KrF laser discharge experiments. The cavity was filled with a 2 atm mix of 93.7% Ar, 6% Kr and 0.3% F_2. Figure 20 shows the experimental results and theoretical predictions when the 0.3 μF capacitor is charged to 10 kV. The top trace is the discharge voltage. The second trace is the discharge current. The third trace is the KrF^* fluorescence. By the end of the pulse the enhancement in the fluorescence is 3. The metastables are being produced with a maximum efficiency of 1.4 times the efficiency of metastable production by a pure e-beam. Figure 21 shows

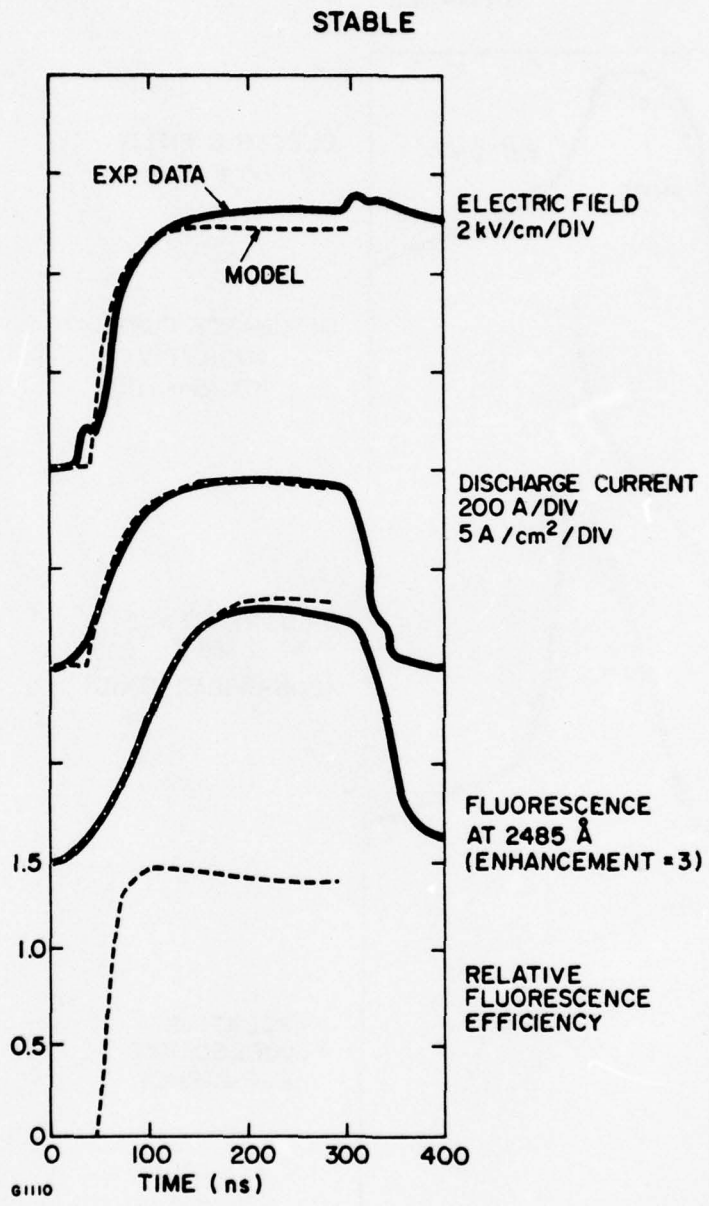

Figure 20 Measured and Predicted Fluorescence When the Capacitor is Charged to 10 kW. The discharge cavity contained 2 atm of 93.7% Ar, 6% Kr and 0.3% F_2

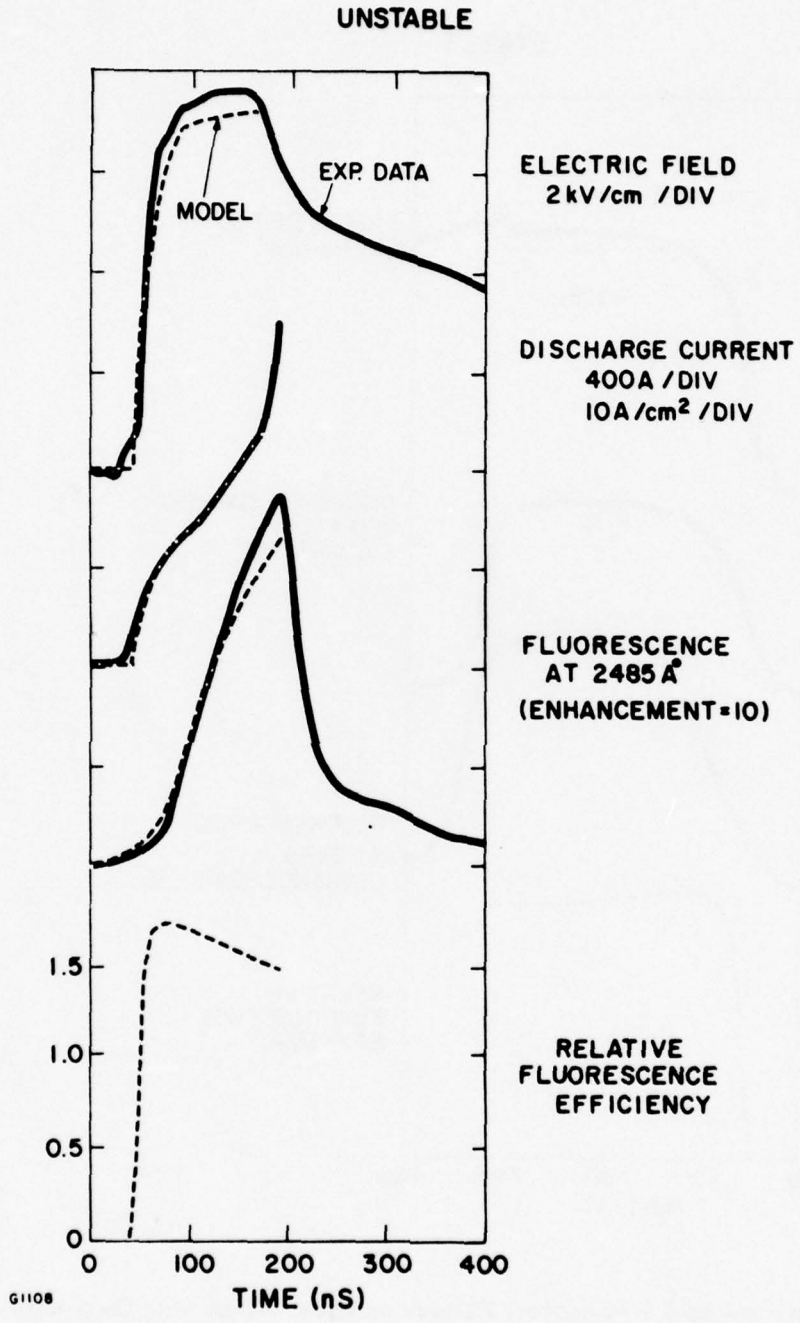

Figure 21 Measured and Predicted Fluorescence When the Capacitor is Charged to 16 kV. The discharge cavity contained 2 atm of 93.7% Ar, 6% Kr, and 0.3% F_2

the results when the capacitor is charged to 16 kV. In this case the discharge current continually increases until the discharge goes through the glow to arc transition which is marked by an abrupt decrease in KrF^* fluorescence. We believe that the initial (slow) increase in the discharge current is caused by a volumetric discharge instability discussed previously. The efficiency for producing the metastables rises rapidly to 1.7 times the efficiency of producing metastables in a pure e-beam and then begins to fall despite the fact that the voltage is constant. The KrF^* production efficiency decreases because as the metastable density increases and the discharge pumping efficiency of Ar^* and Kr^* falls.

V. POWER EXTRACTION

The power extracted from a laser cavity with a well saturated gain medium was analyzed by Rigrod.[49] In his analyses he assumed a stable optical resonator homogeneously broadened gain coefficient, and plain electromagnetic waves. He also assumed steady state conditions and includes mirror losses. Rigrod model has been extended to account for a distributed absorption in the active medium.[50] Such a modification is necessary because of the excited state and molecular ion absorption at the laser wavelengths as will be discussed subsequently. For this case the extraction efficiency can be presented as a function of the small signal gain, g_o, absorption coefficient, α, the laser length, L, the saturation flux, ϕ_{sat}, and the reflectivity of the mirrors. The steady state analysis is valid provided the laser pulse is much longer than the gain rise time and photon transit time through the laser cavity. So this analysis will be applicable for the μsec laser pulses obtained by e-beam and e-beam controlled discharge pumping. The analysis is not valid for the short pulses typical of the UV preionized lasers.

A. POWER EXTRACTION IN KrF^*

Figure 22 shows the variation of the optimum extraction efficiency, as a function of the small signal gain, $g_o L$, for various intrinsic absorption αL. The efficiency is calculated for the optimum mirror reflectivity (output coupling) and it is assumed that the lower laser level is repulsive (as in KrF^*).

(49) W.W. Rigrod, J. Appl. Phys. 36, 2487 (1965).

(50) J.A. Mangano, AERL, to be published.

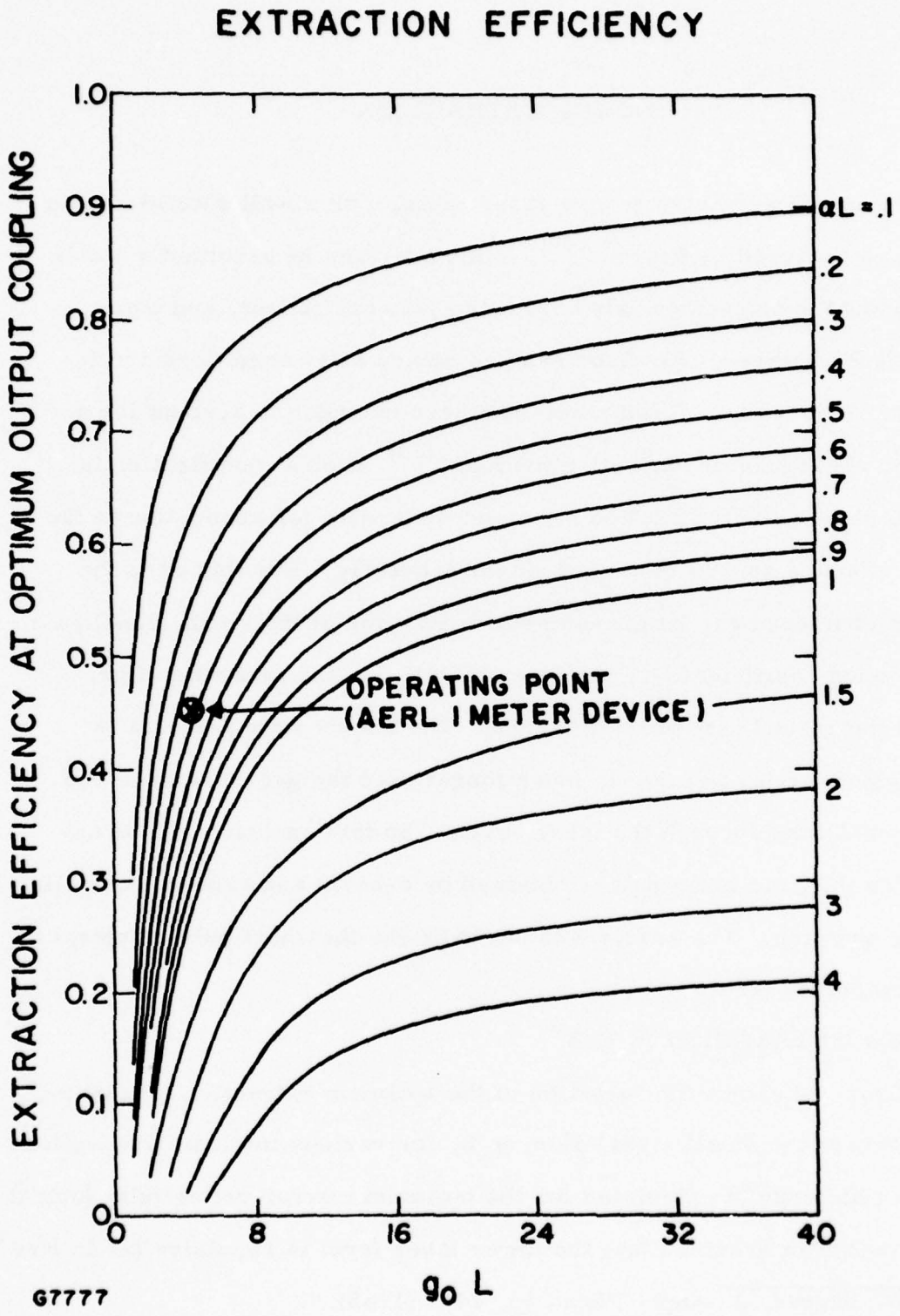

Figure 22 Extraction Efficiency at Optimum Output Coupling as a Function of goL

An important feature of these curves is that a laser that has intrinsic absorption cannot be scaled in length indefinitely. For example, for a $g_o L$ of 8 and an αL of 0.5, the extraction efficiency is 55%. If the length is increased a factor of 5 so $g_o L$ is 40 and αL is 2.5, the extraction efficiency drops to 33%.

Absorption in the active media has been investigated.[51] There are a number of species that can photoabsorb at 249 nm. Stuenenberg and Vogel[52] have determined that the F_2 photoabsorption cross-section is about 1.3×10^{-20} cm^2. By probing an e-beam excited mixture with a flashlamp pumped dye laser, broadband absorption has been observed.[51] This absorption can be explained as contributions from positive and negative ionic states (Ar_2^+, Kr_2^+, F^-), by triatomic species such as Kr_2F^* and by the high lying rare gas electronic states Ar^{**} (4p states). Table 4 lists the dominant absorpting species and their respective cross-sections at 249 nm (other than F_2). This table also gives the number densities of these species as predicted from our kinetic code for 1.5 A/cm^2 and 6 A/cm^2 e-beam current densities.

The F^- photodetachment cross-section has been measured by Mandl[53] between 245 and 270 m. The photoionization cross-sections of Ar^{**} and Kr^{**} (4p and 5p states respectively) have been calculated by H. Hyman.[54] Stevens,

(51) A. M. Hawryluk, J. A. Mangano and J. H. Jacob, "Gain and Absorption Measurements in a KrF* Laser," Appl. Phys. Lett. 31, 164-166 (1977).

(52) R. K. Stuenenberg and R. C. Vogel, J. Am. Chem. Soc. 78, 901- (1976).

(53) A. Mandl, "Electron Photodetachment Cross-section of the Negative Ion of Fluorine," Phys. Rev. A3, 251-255 (1970).

(54) H. A. Hyman, "Photoionization Cross-sections for Excited States of Argon and Krypton," Appl. Phys. Lett. 31, 14-15 (1977).

TABLE 4

KrF* PHOTOABSORPTION

SPECIE	PHOTOABSORPTION CROSS SECTION cm^2	SOURCE	NUMBER DENSITY cm^{-3}		ABSORPTION cm^{-1}	
			1.5 A/cm^2	6 A/cm^2	1.5 A/cm^2	6 A/cm^2
F^-	5.6×10^{-18}	MANDL	1.1×10^{14}	2.2×10^{14}	6.2×10^{-4}	1.2×10^{-3}
Kr_2^+	1.6×10^{-18}	ESTIMATED	4.3×10^{13}	4.9×10^{13}	6.9×10^{-5}	7.9×10^{-5}
Kr_2F^*	1.6×10^{-18}	ESTIMATED	3.7×10^{14}	1.5×10^{15}	5.9×10^{-4}	2.4×10^{-3}
Ar_2^+	1.3×10^{-17}	STEVENS ET AL	5.3×10^{12}	1.8×10^{13}	6.9×10^{-5}	2.3×10^{-4}
Ar^{**}, Kr^{**}	6×10^{-18}	HYMAN	6.2×10^{12}	2.6×10^{13}	3.7×10^{-5}	1.6×10^{-4}
TOTAL CALCULATED ABSORPTION					1.4×10^{-3}	4.1×10^{-3}
TOTAL MEASURED ABSORPTION					1.5×10^{-3}	4.4×10^{-3}

G8167-1

Gardner and Karo[55] and Wadt and Hay[56] have recently calculated the Ar_2^+ photodissociation cross-section ($^2\Sigma_u^+ \rightarrow {}^2\Sigma_g^+$). The Kr_2^+ photoabsorption cross-section was estimated by red shifting Ar_2^+ cross-section as given by Stevens, Garder and Karo[55] by 20 nm. Finally we have assumed that Kr_2F^* will have the same absorption cross-section as Kr_2^+.[54] The total absorption measured at an e-beam current density of 1.5 A/cm^2 is 1.5×10^{-3} cm^{-1}. From the data listed in Table 4 we calculate an absorption of 1.4×10^{-3} cm^{-1}. At 6 A/cm^2 the measured and calculated values are 4.4×10^{-3} cm^{-1} and 4.1×10^{-3} cm^{-1} respectively.

The gain on line center has also been measured. From the gain and absorption measurements the stimulated emission cross-section is 2.5 ± 0.3 Å^2. Tellinghuisen et al[58] have analyzed the KrF^* spontaneous emission spectrum and found a value of 2.6 ± 0.3 Å^2. From these results we can conclude that the self-absorption of the KrF^* to the Rydberg levels is negligible.

The above results have been used to predict the performance of KrF^* on the one-meter AERL device. The best result by pure e-beam pumping are listed in Table 5. For these conditions $g_o L = 3.7$, $\alpha L \approx 0.35$ and the predicted extraction efficiency is 46%. This corresponds to a computed intrinsic efficiency of 9.8% compared to the measured efficiency of 9%. The optical energy extracted was 102 J in 8.5 liters corresponding to an energy density of 12 J/liter.

---

(55) Walter J. Stevens, Maureen Gardner and Arnold Karo, "Theoretical Determination of Bound-Free Absorption Cross-sections in Ar_2^+," J. Che. Phys. 67, 280-2867 (1977).

(56) Willard R. Wadt, David C. Cartwright and James S. Cohen, "Theoretical Absorption Spectra for Ne_2^+, Ar_2^+, Kr_2^+, and Xe_2^+ in the Near Ultraviolet," Appl. Phys. Lett. 31, 672-674 (1977).

(57) M. Krauss, NBS, private communication.

(58) J. Tellingheusen, A.K. Hays, J.M. Hoffman and G.C. Tiscone, J. Chem. Phys. 65, 4473 (1976).

TABLE 5. PERFORMANCE: E-BEAM PUMPED KrF LASER
(0.2% F_2/4% Kr/95.8% Ar AT 1.7 ATM)

- **LASER PERFORMANCE**
  - LASER ENERGY = 102 JOULES
  - ACTIVE VOLUME = 8.5 LITERS
  - LASER ENERGY DENSITY = 12 J/LITER
  - LASER ENERGY/ENERGY DEPOSITED = 9%
  - LASER PULSE LENGTH = 600 nsec
- **E-BEAM CHARACTERISTICS**
  - BEAM CURRENT DENSITY = 11.5 A/cm^2
  - BEAM ENERGY = 250 keV

G9332

Finally, the best laser results obtained by e-beam controlled discharge pumping are summarized in Table 6. These results are limited by the fact that the discharge is unstable for electric fields greater than 2 kV/atm. Ideally, we would like to operate at electric fields of 3 kV/cm atm. At such electric field strengths, both the discharge enhancement and intrinsic efficiency would be higher. Theoretically the efficiency should increase to 15% and the enhancement to 4. The unstable discharge is probably the result of nonuniformities in the ionization produced by the fast electrons. The stability criteria applies to the region of largest input power; hence, a non-uniform discharge will not be as stable as a uniform discharge.

B. POWER EXTRACTION IN XeF^*

The best performance of the XeF^* laser by e-beam pumping is listed in Table 6. These results were obtained in a Ne-rich mixture. The experimental efficiency of 2.6% is less than 1/2 that of KrF^*. In part the decreased efficiency is because of the lower quantum efficiency. In Ne-rich mixtures the finite relaxation time of the upper manifold and the bound lower level decreases the maximum obtainable efficiency as will be discussed in this section. In Ar-rich mixtures the active medium absorption further decreases the extraction efficiency.

The dominant absorbing species in e-beam pumped XeF^* gas mixtures have been identified by systematic absorption measurements.[59] The measured and calculated absorption cross-sections of the different species are listed in Table 7. In Figure 23 a comparison of the absorption in Ar and Ne-rich mixtures is shown. These mixtures contained 0.5% Xe and 0.2% F_2.

(59) M. Rokni, J.H. Jacob, J.A. Mangano and R. Brochu (unpublished).

TABLE 6. E-BEAM CONTROLLED DISCHARGE PUMPING OF KrF^*
1 METER DEVICE (0.5% F_2/10% Kr/89.5% Ar AT 1.5 ATM)

- **LASER PERFORMANCE**
  - LASER ENERGY = 75 JOULES
  - ACTIVE VOLUME = 7.5 LITERS
  - LASER ENERGY DENSITY = 10 J/LITER
  - LASER ENERGY/ENERGY DEPOSITED = 9.5%
  - LASER PULSE LENGTH = 500 nsec
  - OUTPUT COUPLING = 71%

- **DISCHARGE CHARACTERISTICS**
  - DISCHARGE ELECTRIC FIELD $\simeq$ 2 kV/cm–atm
  - DISCHARGE CURRENT DENSITY = 70 A/cm^2
  - DISCHARGE ENERGY DEPOSITED = 70 J/LITER

- **E–BEAM CHARACTERISTICS**
  - BEAM CURRENT DENSITY = 4 A/cm^2
  - BEAM ENERGY = 300 keV
  - BEAM ENERGY DEPOSITED = 35 J/LITER

H1887

TABLE 7

SPECIES	σ cm^2 300 ^{0}K	
	EXP.	THEOR.
Ar_2^+	1.7×10^{-17}	2×10^{-17} (REF 5) 8.7×10^{-18} (REF 6)
Xe_2^+	1.2×10^{-16}	4.8×10^{-17} (REF 6)
Ne_2^+	–	9.6×10^{-19} (REF 6)

H 2014

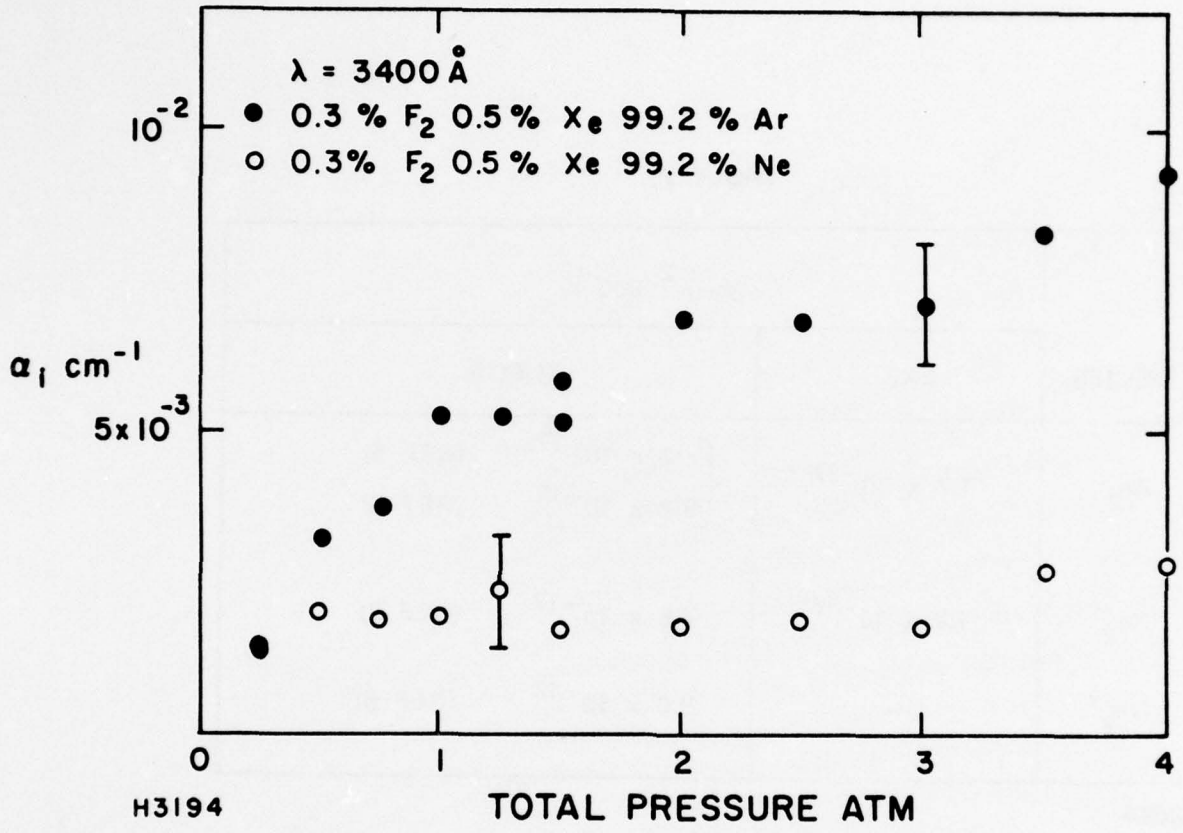

Figure 23 Excited State Absorption in $Ar/Xe/F_2$ and $Ne/Xe/F_2$ Mixtures

From this figures it is apparent that in $Ne/Xe/F_2$ mixtures the observed photoabsorption is much less.[60] The two main reasons for the decreased photoabsorption in Ne-rich mixtures at XeF wavelengths are (1) Ne_2^+ photoabsorption at XeF wavelengths is much smaller than Ar_2^+ photoabsorption and (2) Xe_2^+ formation is much slower because the intermediate complex $NeXe^+$, in contrast to $ArXe^+$, is probably only weakly bound or unbound.[61]

Figure 24 shows the bound upper and lower XeF laser levels. The dominant laser transition is the $v' = 0 \rightarrow v'' = 3$ (353 nm). The extraction efficiency will depend on the lower level lifetime and the vibrational relaxation rate of the upper manifold. Starting with rate equations for the upper and lower levels it can be shown that extraction efficiency is given by[62]

$$\eta_{ext} = \eta \left(\frac{\Theta \tau_u/\tau_v}{1 + \Theta \tau_u/\tau_v} \right) \lim_{\phi \gg \phi_s} \left[1 - \frac{N^*(v=0)}{N_0^*(v=0)} \right] \qquad (23)$$

where η is the extraction efficiency plotted in Figure 22. The second term accounts for the finite vibrational relaxation time of the upper laser manifold. Θ is the fractional population in $v = 0$ under the equilibrium conditions, τ_u is the upper level lifetime and τ_v is the vibrational relaxation time. When $\Theta\tau_u/\tau_v \gg 1$ this term approaches unity. The last term accounts for the inefficiency resulting from finite lifetime of the lower laser level ($v'' = 3$). For a repulsive lower level, as in the case of KrF^* this limit is unity.

We will first consider the effect of the vibrational relaxation of the upper manifold. In Ar-rich mixtures, as we have discussed previously, the vibrational relaxation is faster than in Ne-diluted mixtures. The second term

(60) L. F. Champagne and N. W. Harris, "The Influence of Diluent Gas on the XeF Laser," Appl. Phys. Lett. 31, 513-515 (1977).

(61) M. Krauss, NBS, private communication.

(62) M. Rokni, AERL, private communication.

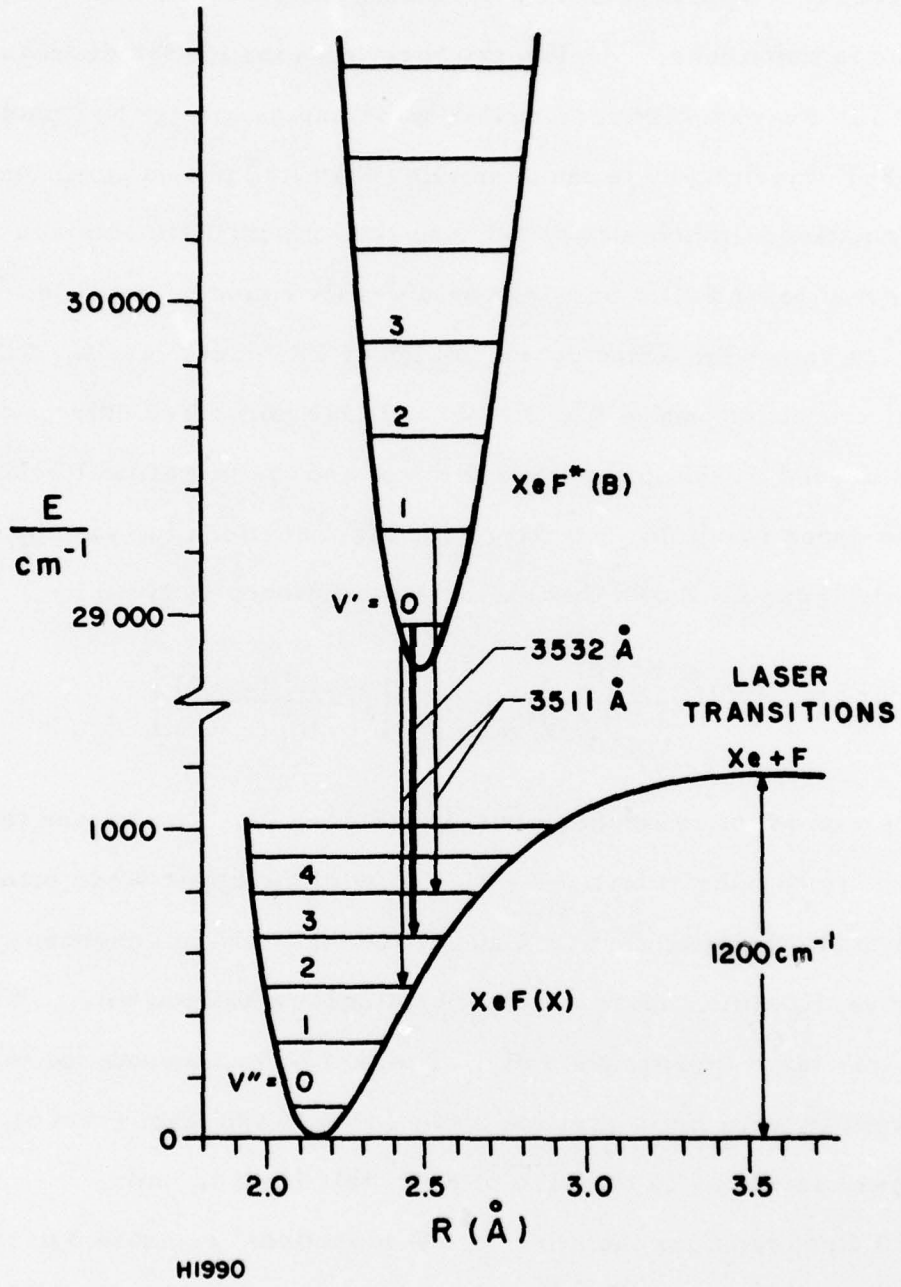

Figure 24 Schematic Showing the Upper and Lower Levels of XeF*

in Eq. (23) is unity when Ar is used as a buffer. The same is true in the KrF laser mixtures of $Ar/Kr/F_2$. Figure 25 shows time integrated side light spectra of XeF in a $Ne/Xe/NF_3$ mixture for lasing and non-lasing conditions. From this figure it is evident that the laser radiation depresses only the $v' = 0$ population density while the higher vibrational levels are not affected. As a result, the second term in Eq. (23) is about 0.6, i.e., 60% of the available energy can be extracted.

In contrast to KrF^* the lower level of XeF^* is bound by about 0.15 eV. In steady state at ambient temperature and typical laser mixture pressures, most of the XeF will dissociate into Xe + F. However, if the dissociation rate τ_D is comparable or slower than the upper level lifetime, the extraction efficiency will be decreased by the third term of Eq. (23). Figure 26 shows the side light emission at 353.2 nm ($v' = 0 \rightarrow v'' = 3$) under lasing and non-lasing conditions. Under lasing conditions we ensured that the cavity flux was at least an order of magnitude larger than the saturation flux. From the side light fluorescence the ratio of $N^*(v = 0)/N_0^*(v = 0)$ in the limit $\phi/\phi_s \gg 1$ is determined to be ≈ 0.6. Therefore, the last term of Eq. (23) is 0.4. The decrease in the extraction due to the lower level can be understood from the schematic diagram shown in Figure 27. For a repulsive lower level if $\phi_s/\phi = 10$, the side light will be depressed by a factor of 11. For this condition a finite $\Delta N = N^* - N$ required to overcome the cavity loss. In the case of a repulsive lower level $N = 0$, hence $N^* = \Delta N$. For a bound lower level and steady state lasing conditions, the population of the ground state will be finite and dependent on the ground state lifetime. For the same cavity loss (same ΔN) $N^* = N + \Delta N$ to sustain lasing action. Hence the extraction efficiency is lower by the factor given in Eq. (23).

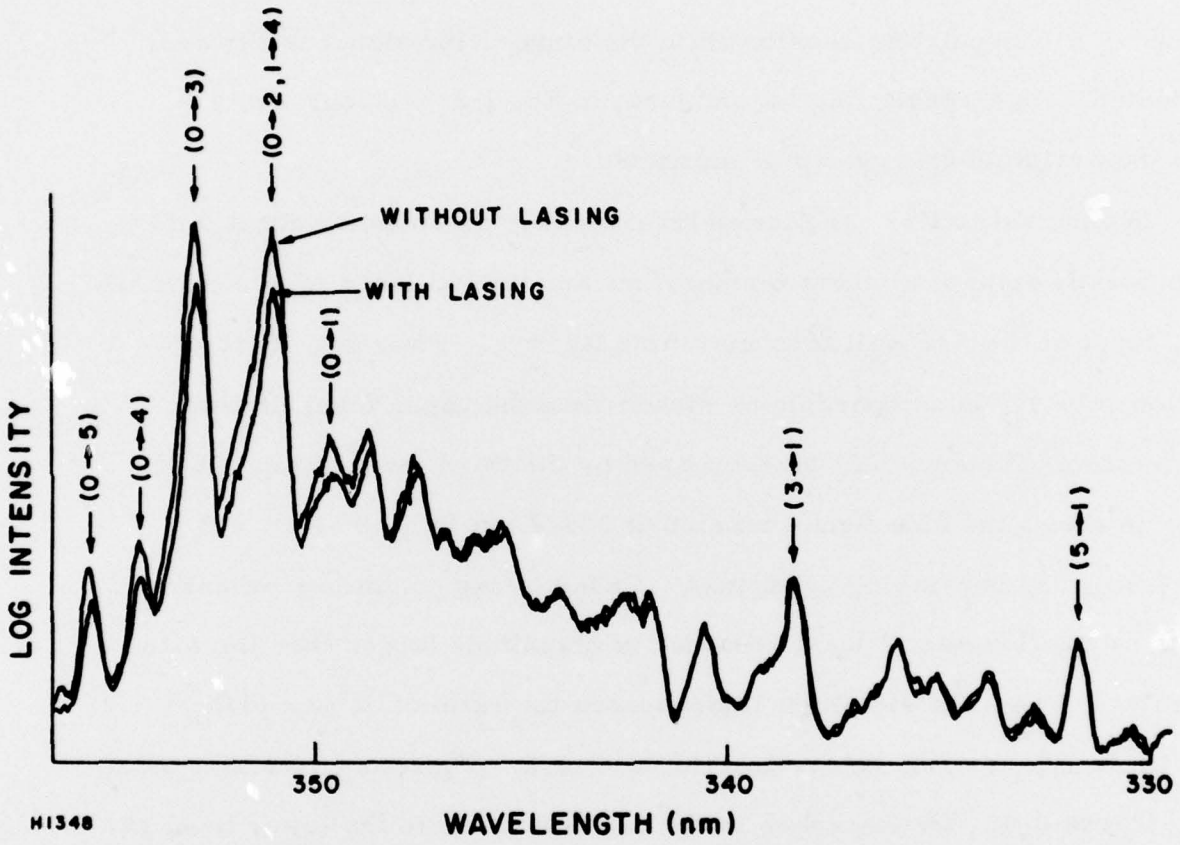

Figure 25 XeF* Sidelight Spectra With and Without Lasing

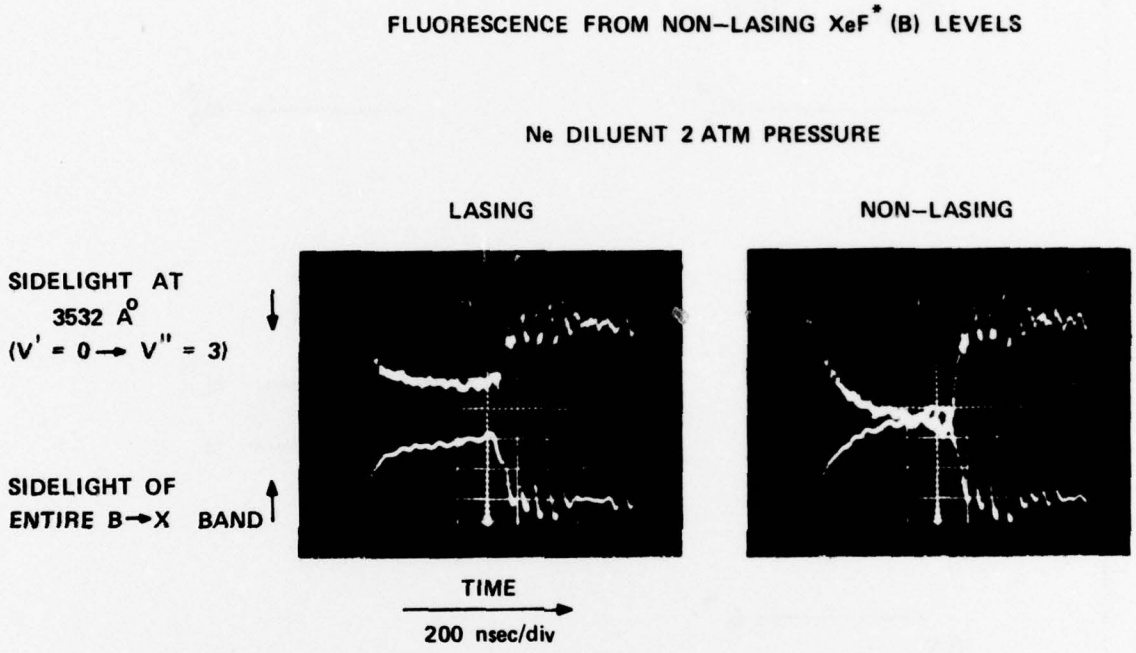

Figure 26 XeF* Sidelight Emission at 353. 2 nm With and Without Lasing

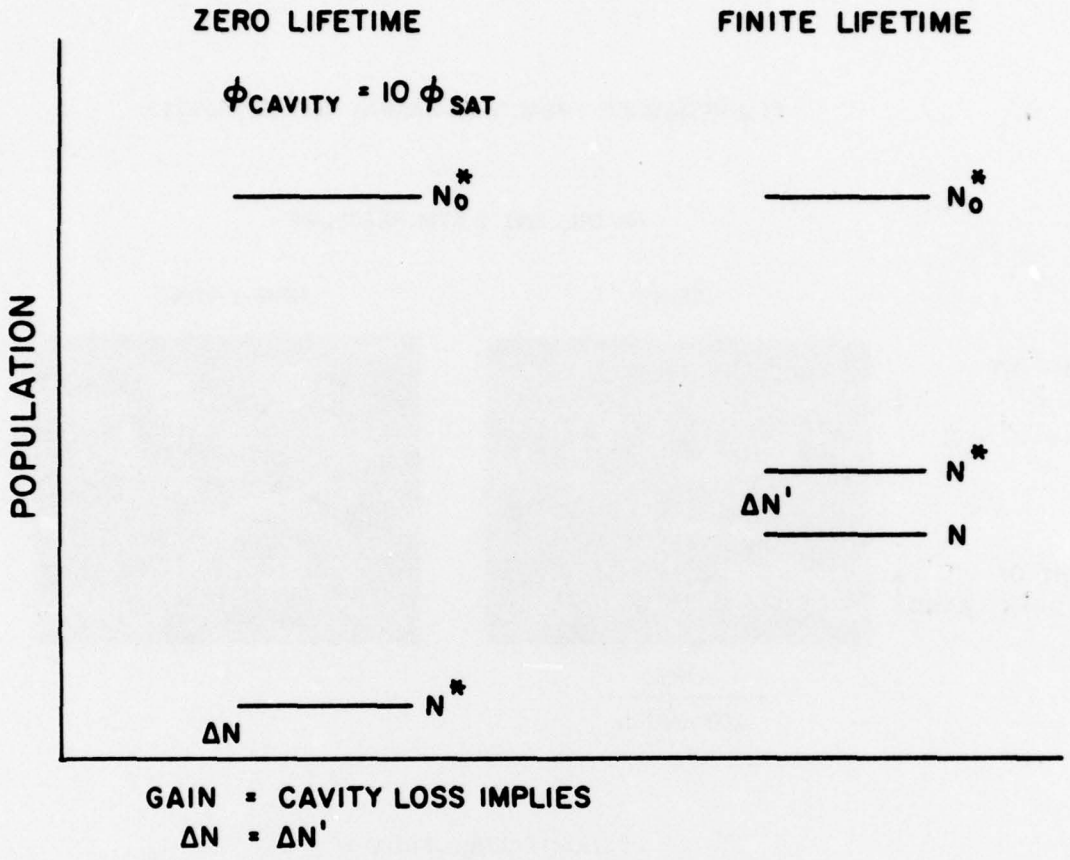

$$\frac{dN^*}{dt} = S - \frac{\sigma_{STIM}}{h\nu}\,\Delta N\phi - \frac{N^*}{\tau} = 0$$

$$\text{EXTRACTION EFFICIENCY} = \frac{\sigma_{STIM}\,\Delta N\phi}{h\nu S}$$

$$= 1 - \frac{N^*}{N_0^*} = 0.4$$

H1560

Figure 27 Schematic Showing the Effects of a Lower Laser Level Having a Finite Life Time

VI. CONCLUSION

The rare gas fluoride lasers can be very efficient and have the potential of being scaled to high average powers. To date the best efficiencies and single pulse energies have been obtained from KrF^* which has a repulsive lower level. The formation, quenching and extraction of the KrF^* laser is understood well enough to enable laser performance predictions. In the XeF^* laser the physics is more complicated. It appears that the efficiency is constrained by the bound lower level, the finite vibrational relaxation of the upper level and intrinsic active medium absorption. The intrinsic absorption is greatly reduced by using Ne as a buffer instead of Ar; however, in the presence of Ne the vibrational relaxation of the upper laser level is slower than in the presence of Ar.

New families of exciplex lasers having ionic upper levels, as in the rare gas fluorides, can be researched. The mercury monohalides discovered recently is an example of such a class of lasers. As in the case of the rare gas halides these exciplexes were first lased by pure e-beam pumping.[6] Laser action has also been obtained by e-beam controlled discharge pumping.[63] The mercury monohalide lasers radiate in the visible and have the potential of achieving high power and efficiencies. There are also triatomic exciplexes analogous to the rare gas halides that could possibly lase. These systems will be far more complex with a high density of states and numerous curve crossings and hence the probability of achieving efficient lasing is expected to be smaller than in the diatomic exciplexes.

(63) J.H. Jacob, J.A. Mangano, M. Rokni and B.N. Srivastava, presented at the 20th Gaseous Electronic Conf., Oct. (1977); M. McCusker etal ibid, W. Watt private communication.

REFERENCES

1. J.E. Velazco and D.W. Setser, "Quenching of Xe Metastable Atoms," JQE 11, 708-709 (1975).

2. M.C. Golde and B.A. Thrush, Chem. Phys. Lett. 29, 486 (1974).

3. S.K. Searles and G.A. Hart, "Stimulated Emission at 281.8 nm from XeBr," Appl. Phys. Lett. 27, 243-245(1975).

4. J.J. Ewing and C.A. Brau, "Laser Action on the $^2\Sigma^+_{1/2} \rightarrow {}^2\Sigma^+_{1/2}$ Bands of KrF and XeCl," Appl. Phys. Lett. 27, 350-252 (1975).

5. C.A. Brau and J.J. Ewing, "354 nm Laser on XeF," Appl. Phys. Lett. 27, 435-437 (1975).

6. J.H. Parks, "Laser Action on the $B^2\Sigma^+_{1/2} \rightarrow X^2\Sigma^+_{1/2}$ Band of HgCl at 5576 Å," Appl. Phys. Lett. 31, 192-194 (1977).

7. J.J. Ewing, private communication (1976).

8. J.A. Mangano and J. Hsia, "Interim Report - One Meter KrF^* Laser," Semi-Annual Technical Report, Aug. 76 - Feb. 77.

9. J.A. Mangano and J.H. Jacob, "E-beam Controlled Discharge Pumping of the KrF^* Laser," Appl. Phys. Lett. 27, 495-498 (1975).

10. J.A. Mangano and J. Hsia, "Interim Report - One Meter KrF^* Laser," Semi-Annual Technical Report, Feb. 77 - Aug. 77.

11. R. Burnham, H.W. Harris and N. Djeu, "Xenon Fluoride Laser Excitation by Transverse Electric Discharge," Appl. Phys. Lett. 28, 86-87 (1976).

12. C.P. Wang, H. Mirles, D.G. Sutton and S.N. Suchard, "Fast Discharge Initiated XeF Laser," Appl. Phys. Lett. 28, 326-328, (1976).

13. J.A. Mangano, J.H. Jacob, M. Rokni and A. Hawryluk, "Three Body Quenching of KrF^* by Ar and Broadband Emission at 415 nm," Appl. Phys. Lett. 31, 26-28 (1977).

14. M. Rokni, J.H. Jacob, J.A. Mangano and R. Brochu, "Two and Three Body Quenching of XeF^* by Ar and Xe," Appl. Phys. Lett. 30, 458-460 (1977).

15. J.H. Jacob and J.A. Mangano, "Modeling of the KrF Laser Discharge," Appl. Phys. Lett. 28, 724-726 (1976).

16. E. W. McDaniel, V. Cermak, A. Dalgarno, E. E. Ferguson and L. Friedman, "Ion-Molecule Reactions," (Wiley-Interscience, New York, 1970) pp. 338-339.

17. D. K. Bohme, N. G. Adams, M. Moselman, D. B. Dunkin and E. E. Ferguson, "Flowing Afterglow Studies of the Reactions of the Rare-Gas Molecular Ions He_2^+, Ne_2^+ and Ar_2^+ with Molecules and Rare-Gas Atoms," J. Chem. Phys. 52, 5904 (1970).

18. Thom. H. Duning and P. Jeffrey Hay, "Electronic States of KrF," Appl. Phys. Lett. 28, 649-651 (1976).

19. S. R. LaPaglia and A. B. F. Duncan, J. Chem. Phys. 34, 1003 (1961).

20. M. Rokni, J. H. Jacob and J. A. Mangano, "Formation Processes in E-beam Pumped Ne/Xe/F_2 Mixtures," Appl. Phys. Lett. to appear in Feb. (1978).

21. Dunning & Hay, LASL, private communication.

22. Measurements by D. K. Bohme, N. G. Adams, M. Moselman, D. B. Dunkin and E. E. Ferguson, in Ref. 17 show that the rate constant for $Ne_2^+ + Kr \rightarrow Kr^+ + 2Ne$ and $Ne_2^+ + Ar \rightarrow Ar^+ + 2Ne$ is very slow, ($< 5 \times 10^{-13}$ cm^3/sec). So it is reasonable to expect that the charge transfer from $Ne_2^+ \rightarrow Xe^+$ will not be dominant in e-beam pumped XeF laser mixtures.

23. C. A. Brau and J. J. Ewing, "Emission Spectra of XeBr, XeCl, XeF and KrF*," J. Chem. Phys. 63, 4640-4647 (1975).

24. M. Krauss, NBS private communication.

25. J. A. R. Samson and K. L. Kelley, C. C. A. Tech. Rept. No. 69-3-N (1964).

26. M. Krauss, NBS, private communication.

27. C. H. Chen, J. P. Judish and M. G. Payne, "Energy Transfer Process in Ar-Xe and Ar-F_2 Mixtures" (unpublished).

28. L. G. Piper, J. E. Velazco and D. W. Setser, J. Chem. Phys. 59, 3323 (1973).

29. M. Bourene, O. Dutnuit and J. LeCalve, J. Chem. Phys. 63, 1668 (1975).

30. J. E. Velazco, J. H. Kolts and D. W. Setser, J. Chem. Phys. 65, 3468 (1976).

31. M. Rokni, J. H. Jacob, J. A. Mangano and R. Brochu, "Formation and Quenching Kinetics of ArF," Appl. Phys. Lett. 31, 79-82, (1977).

32. J.H. Jacob, M. Rokni and J.A. Mangano, Semi-Annual Technical Report for period March 1975 to September 1976.

33. J.H. Jacob, M. Rokni, J.A. Mangano and R. Brochu, "Formation and Quenching Processes in Kr/F_2 Mixtures," to appear Appl. Phys. Lett. Jan (1978).

34. J.D. Daugherty, E.R. Pugh, and D.H. Douglas-Hamilton, Bull. Am. Phys. Soc. 16, 399 (1971); C.A. Fernsternmacher, M.J. Nutter, J.P. Rink and K. Boyer, Bull. Am. Phys. Soc. 16, 42 (1971).

35. H.A. Koehler, L.J. Ferderber, D.L. Redhead and D.J. Ebert, Appl. Phys. Lett. 21, 198 (1972); PρW. Hoff, J.C. Swingle and C.K. Rhodes, Appl. Phys. Lett. 23, 245 (1973).

36. K. Boyer, D.B. Henderson and R.L. Morse, J. Appl. Phys. 44, 5511 (1973).

37. J.A. Mangano, AERL (unpublished).

38. H.A. Bethe, M.E. Rose, L.P. Smith, Proc. Am. Philos. Soc. 89, 1256 (1938).

39. J.H. Jacob, J. Appl. Phys. 45, 467 (1974).

40. H.A. Bethe and J.H. Jacob, "Diffusion of Fast Electrons in the Presence of an Electric Field," Phys. Rev. A16, 1952 (1977).

41. J.H. Jacob, "Diffusion of Fast Electrons in the Presence of a Magnetic Field," Appl. Phys. Lett. 31, 252-254 (1977).

42. H. Hyman, AERL private communication.

43. R.H. McFarland and J.D. Kinney, Phys. Rev. 137, 1058 (1965).

44. J.H. Jacob and J.A. Mangano, "Total Electron Impact Excitation Cross Sections of Ar and Kr," Appl. Phys. Lett. 29, 467-469 (1976).

45. D. Rapp and P. Englander-Golden, J. Chem. Phys. 43, 1464 (1965).

46. Recent calculations by W.H. Long, Jr., "Electron Kinetics in the KrF Laser," Appl. Phys. Lett. 31, p. 391-394 (1977) have shown that electron - electron collisions will effect the discharge kinetics for a reduced electric field of $< 10^{-16}$ V-cm^2 and fractional electron densities of $>10^{-5}$. Similar calculations have also been performed by William H. Nyhan of United Technologies. The discharge data presented in the following sections are for electric fields $> 10^{-16}$ V-cm^2 and maximum fractional electron densities $\leq 2 \times 10^{-5}$. For these conditions electron-electron collisions will have a 10% effect on the discharge kinetics.

47. J. D. Daugherty, J. A. Mangano, and J. H. Jacob, "Attachment-Dominated E-beam Ionized Discharges," Appl. Phys. Lett. 28, 581-582 (1976).

48. J. C. Hsia, "A Model for Preionization in Electric-Discharge Pumped XeF and KrF Lasers," Appl. Phys. Lett. 30, pp. 101-103 (1977).

49. W. W. Rigrod, J. Appl. Phys. 36, 2487 (1965).

50. J. A. Mangano, AERL, to be published.

51. A. M. Hawryluk, J. A. Mangano and J. H. Jacob, "Gain and Absorption Measurements in a KrF* Laser," Appl. Phys. Lett. 31, 164-166 (1977).

52. R. K. Stuenenberg and R. C. Vogel, J. Am. Chem. Soc. 78, 901- (1956).

53. A. Mandl, "Electron Photodetachment Cross Section of the Negative Ion of Fluorine," Phys. Rev. A3, 251-255 (1970).

54. H. A. Hyman, "Photoionization Cross Sections for Excited States of Argon and Krypton," Appl. Phys. Lett. 31, 14-15 (1977).

55. Walter J. Stevens, Maureen Gardner and Arnold Karo, "Theoretical Determination of Bound-Free Absorption Cross Sections in Ar_2^+," J. Chem. Phys. 67, 280-2867 (1977).

56. Willard R. Wadt, David C. Cartwright and James S. Cohen, "Theoretical Absorption Spectra for Ne_2^+, Ar_2^+, Kr_2^+, and Xe_2^+ in the Near Ultraviolet," Appl. Phys. Lett. 31, 672-674 (1977).

57. M. Krauss, NBS, private communication.

58. J. Tellingheusen, A. K. Hays, J. M. Hoffman and G. C. Tiscone, J. Chem. Phys. 65, 4473 (1976).

59. M. Rokni, J. H. Jacob, J. A. Mangano and R. Brochu (unpublished).

60. L. F. Champagne and N. W. Harris, "The Influence of Diluent Gas on the XeF Laser," Appl. Phys. Lett. 31, 513-515 (1977).

61. M. Krauss, NBS, private communication.

62. M. Rokni, AERL, private communication.

63. J. H. Jacob, J. A. Mangano, M. Rokni and B. N. Srivastava, presented at the 20th Gaseous Electronic Conf., Oct. (1977); M. McCusker etal ibid, W. Watt private communication.

DISTRIBUTION LIST

Office of Naval Research, Department of the Navy, Arlington, VA 22217 - Attn: Physics Program (3 copies)

Naval Research Laboratory, Department of the Navy, Washington, D.C. 20375 - Attn: Technical Library (1 copy)

Office of the Director of Defense, Research and Engineering, Information Office Library Branch, The Pentagon, Washington, D.C. 20301 (1 copy)

U.S. Army Research Office, Box CM, Duke Station, Durham, N.C. 27706 (1 copy)

Defense Documentation Center, Cameron Station, Alexandria, VA 22314 (12 copies)

Defender Information Analysis Center, Battelle Memorial Institute, 505 King Avenue, Columbus, OH 43201 (1 copy)

Commanding Officer, Office of Naval Research Branch Office, 536 South Clark Street, Chicago, IL 60615 (1 copy)

New York Area Office, Office of Naval Research, 715 Broadway (5th Floor), New York, NY 10003 - Attn: Dr. Irving Rowe (1 copy)

San Francisco Area Office, Office of Naval Research, 760 Market Street, Room 447, San Francisco, CA 94102 (1 copy)

Air Force Office of Scientific Research, Department of the Air Force, Washington, D.C. 22209 (1 copy)

Office of Naval Research Branch Office, 1030 East Green Street, Pasadena, CA 91106 - Attn: Dr. Robert Behringer (1 copy)

Code 102 1P (ONRL), Office of Naval Research, 800 N. Quincy Street, Arlington, VA 22217 (6 copies)

Defense Advanced Research Projects Agency, 1400 Wilson Blvd., Arlington, VA 22209 - Attn: Strategic Technology Office (1 copy)

Office Director of Defense, Research & Engineering, The Pentagon, Washington, D.C. 20301 - Attn: Assistant Director (Space and Advanced Systems) (1 copy)

Office of the Assistant Secretary of Defense, System Analysis (Strategic Programs), Washington, D.C. 20301 - Attn: Mr. Gerald R. McNichols (1 copy)

U.S. Arms Control and Disarmament Agency, Dept. of State Bldg., Rm. 4931, Washington, D.C. 20451 - Attn: Dr. Charles Henkin (1 copy)

Energy Research Development Agency, Division of Military Applications, Washington, D.C. 20545 (1 copy)

National Aeronautics and Space Administration, Lewis Research Center, Cleveland, OH 44135 - Attn: Dr. John W. Dunning, Jr. (1 copy)
(Aerospace Res. Engineer)

National Aeronautics & Space Administration, Code RR, FOB 10B, 600 Independence Ave., SW, Washington, D.C. 20546 (1 copy)

National Aeronautics and Space Administration, Ames Research Center, Moffett Field, CA 94035 - Attn: Dr. Kenneth W. Billman (1 copy)

Department of the Army, Office of the Chief of RD&A, Washington, D.C. 20310 - Attn: DARD-DD (1 copy)
DAMA-WSM-T (1 copy)

Department of the Army, Office of the Deputy Chief of Staff for Operations & Plans, Washington, D.C. 20310 - Attn: DAMO-RQD - (1 copy)

Ballistic Missile Defense Program Office (BMDPO), The Commonwealth Building, 1300 Wilson Blvd., Arlington, VA 22209 - Attn: Mr. Albert J. Bast, Jr. (1 copy)

U.S. Army Missile Command, Research & Development Division, Redstone Arsenal, AL 35809 - Attn: Army High Energy Laser Programs (2 copies)

Commander, Rock Island Arsenal, Rock Island, IL 61201, Attn: SARRI-LR, Mr. J.W. McGarvey (1 copy)

Commanding Officer, U.S. Army Mobility Equipment R&D Center, Ft. Belvoir, VA 22060 - Attn: SMEFB-MW (1 copy)

Commander, U.S. Army Armament Command, Rock Island, IL 61201 - Attn: AMSAR-RDT (1 copy)

Director, Ballistic Missile Defense Advanced Technology Center, P.O. Box 1500, Huntsville AL 35807 - Attn: ATC-O (1 copy)
ACT-T (1 copy)

Commander, U.S. Army Material Command, Alexandria, VA 22304 - Attn: Mr. Paul Chernoff (AMCRD-T) (1 copy)

Commanding General, U.S. Army Munitions Command, Dover, NH 17801 - Attn: Mr. Gilbert F. Cheanov (AMSMU-R) (1 copy)

Director, U.S. Army Ballistics Res. Lab, Aberdeen Proving Ground, MD 21005 - Attn: Dr. Robert Eichenberger (1 copy)

Commandant, U.S. Army, Air Defense School, Ft. Bliss, TX 79916 - Attn: Air Defense Agency (1 copy)
ATSA-CTD-MS (1 copy)

Commanding General, U.S. Army Combat Dev. Command, Ft. Belvoir, VA 22060 - Attn: Director of Material, Missile Div. (1 copy)

Commander, U.S. Army Training & Doctrine Command, Ft. Monroe, VA 23651 - Attn: ATCD-CF (1 copy)

Commander, U.S. Army Frankford Arsenal, Philadelphia, PA 19137 - Attn: Mr. M. Elnick SARFA-FCD Bldg. 201-3 (1 copy)

Commander, U.S. Army Electronics Command, Ft. Monmouth, NJ 07703 - Attn: AMSEL-CT-L, Dr. R.G. Buser (1 copy)

Commander, U.S. Army Combined Arms Combat Developments Activity, Ft. Leavenworth, KS 66027 (1 copy)

National Security Agency, Ft. Geo. G. Meade, MD 20755 - Attn: R.C. Foss A763 (1 copy)

Deputy Commandant for Combat & Training Developments, U.S. Army Ordnance Center and School, Aberdeen Proving Ground, MD 21005
Attn: ATSL-CTD-MS-R (1 copy)

Commanding Officer, USACDC CBR Agency, Ft. McClellan, AL 36201 - Attn: CDCCBR-MR (Mr. F.D. Poer) (1 copy)

DISTRIBUTION LIST (Continued)

Department of the Navy, Office of the Chief of Naval Operations, The Pentagon 5C739, Washington, D.C. 20350 - Attn: (OP 'N2F3) (1 copy)

Office of Naval Research Branch Office, 495 Summer Street, Boston, MA 02210 - Attn: Dr. Fred Quelle (1 copy)

Department of the Navy, Deputy Chief of Navy Material (Dev.), Washington, D.C. 20360 - Attn: Mr. R. Gaylord (MAT 032B) (1 copy)

Naval Missile Center, Point Mugu, CA 93042 - Attn: Gary Gibbs (Code 5352) (1 copy)

Naval Research Laboratory, Washington, D.C. 20375 - Attn: (Code 5503-EOTPO) (1 copy)
Dr. P. Livingston - Code 5560 (1 copy)
Dr. A. L. Schindler - Code 6000 (1 copy)
Dr. H. Shenker - Code 5504 (1 copy)
Mr. D.J. McLaughlin - Code 5560 (1 copy)
Dr. John L. Walsh - Code 5503 (1 copy)

High Energy Laser Project Office, Department of the Navy, Naval Sea Systems Command, Washington, D.C. 20360 - Attn: Capt. A. Skolnick, USN (PM 22) (1 copy)

Superintendent, Naval Postgraduate School, Monterey, CA 93940 - Attn: Library (Code 2124) (1 copy)

Navy Radiation Technology, Air Force Weapons Lab (NLO), Kirtland AFB, NM 87117 (1 copy)

Naval Surface Weapons Center, White Oak, Silver Spring, MD 20910 - Attn: Dr. Leon H. Schindel (Code 310) (1 copy)
Dr. E. Leroy Harris (Code 313) (1 copy)
Mr. K. Enkenhaus (Code 034) (1 copy)
Mr. J. Wise (Code 047) (1 copy)
Technical Library (1 copy)

U.S. Naval Weapons Center, China Lake, CA 93555 - Atn: Technical Library (1 copy)

HQ USAF (AF/RDPS), The Pentagon, Washington, D.C. 20330 - Attn: Lt. Col. A.J. Chiota (1 copy)

HQ AFSC/XRLW, Andrews AFB, Washington, D.C. 20331 - Attn: Maj. J.M. Walton (1 copy)

HQ AFSC (DLCAW), Andrews AFB, Washington, D.C. 20331 - Attn: Maj. H. Axelrod (1 copy)

Air Force Weapons Laboratory, Kirtland AFB, NM 87117 - Attn: LR (1 copy)
AL (1 copy)

HQ SAMSO (XRTD), P.O. Box 92960, Worldway Postal Center, Los Angeles, CA 90009 - Attn: Lt. Dorian DeMaio (XRTD) (1 copy)

AF Avionics Lab (TEO), Wright Patterson AFB, OH 45433 - Attn: Mr. K. Hutchinson (1 copy)

Dept. of the Air Force, Air Force Materials Lab. (AFSC), Wright Patterson AFB, OH 45433 - Attn: Maj. Paul Elder (LPS) (1 copy)
Laser Window Group

HQ Aeronautical Systems Div., Wright Patterson AFB, OH 45433 - Attn: XRF - Mr. Clifford Fawcett (1 copy)

Rome Air Development Command, Griffiss AFB, Rome, NY 13440 - Attn: Mr. R. Urts (OCSE) (1 copy)

HQ Electronics Systems Div. (ESL), L.G. Hanscom Field, Bedford, MA 01730 - Attn: Mr. Alfred E. Anderson (XRT) (1 copy)
Technical Library (1 copy)

Air Force Rocket Propulsion Lab., Edwards AFB, CA 93523 - Attn: B.R. Bornhorst, (LKCG) (1 copy)

Air Force Aero Propulsion Lab., Wright Patterson AFB, OH 45433 - Attn: Col. Walter Moe (CC) (1 copy)

Dept. of the Air Force, Foreign Technology Division, Wright Patterson AFB, OH 45433 - Attn: PDTN (1 copy)

Commandant of the Marine Corps, Scientific Advisor (Code RD-1), Washington, D.C. 20380 (1 copy)

Aerospace Research Labs., (AP), Wright Patterson AFB, OH 45433 - Attn: Lt. Col. Max Duggins (1 copy)

Defense Intelligence Agency, Washington, D.C. 20301 - Attn: Mr. Seymour Berler (DTIB) (1 copy)

Central Intelligence Agency, Washington, D.C. 20505 - Attn: Mr. Julian C. Nall (1 copy)

Analytic Services, Inc., 5613 Leesburg Pike, Falls Church, VA 22041 - Attn: Dr. John Davis (1 copy)

Aerospace Corp., P.O. Box 92957, Los Angeles, CA 90009 - Attn: Dr. G.P. Millburn (1 copy)

Airesearch Manuf. Co., 9851-9951 Sepulveda Blvd., Los Angeles, CA 90009 - Attn: Mr. A. Colin Stancliffe (1 copy)

Atlantic Research Corp., Shirley Highway at Edsall Road, Alexandria, VA 22314 - Attn: Mr. Robert Naismith (1 copy)

Avco Everett Research Lab., 2385 Revere Beach Parkway, Everett, MA 02149 - Attn: Dr. George Sutton (1 copy)
Dr. Jack Daugherty (1 copy)

Battelle Columbus Laboratories, 505 King Avenue, Columbus, OH 43201 - Attn: Mr. Fred Tietzel (STPIAC) (1 copy)

Bell Aerospace Co., Buffalo, NY 14240 - Attn: Dr. Wayne C. Solomon (1 copy)

Boeing Company, P.O. Box 3999, Seattle, WA 98124 - Attn: Mr. M.I. Gamble (2-, 460, MS 8C-88) (1 copy)

Electro-Optical Systems, 300 N. Halstead, Pasadena, CA 91107 - Attn: Dr. Andrew Jensen (1 copy)

ESL, Inc., 495 Java Drive, Sunnyvale, CA 94086 - Attn: Arthur Einhorn (1 copy)

DISTRIBUTION LIST (Continued)

General Electric Co., Space Division, P.O. Box 8555, Philadelphia, PA 19101 - Attn: Dr. R.R. Sigismonti (1 copy)

General Electric Co., 100 Plastics Avenue, Pittsfield, MA 01201 - Attn: Mr. D.G. Harrington (Rm. 1044) (1 copy)

General Research Corp., P.O. Box 3587, Santa Barbara, CA 93105 - Attn: Dr. R. Holbrook (1 copy)

General Research Corp., 1501 Wilson Blvd., Suite 700, Arlington, VA 22209 - Attn: Dr. Giles F. Crimi (1 copy)

Hercules, Inc., Industrial System Dept., Wilmington, DE 19899 - Attn: Dr. R.S. Voris (1 copy)

Hercules, Inc., P.O. Box 210, Cumberland, MD 21502 - Attn: Dr. Ralph R. Preckel (1 copy)

Hughes Research Labs., 3011 Malibu Canyon Road, Malibu, CA 90265 - Attn: Dr. D. Forster (1 copy)

Hughes Aircraft Co., Aerospace Group - Systems Division, Canoga Park, CA 91304 - Attn: Dr. Jack A. Alcalay (1 copy)

Hughes Aircraft Co., Centinela and Teale Streets, Bldg. 6, MS E-125, Culver City, CA 90230 - Attn: Dr. William Yates (1 copy)

Institute for Defense Analyses, 400 Army-Navy Drive, Arlington, VA 22202 - Attn: Dr. Alvin Schnitzler (1 copy)

Johns Hopkins University, Applied Physics Lab., 8621 Georgia Avenue, Silver Spring, MD 20910 - Attn: Dr. Albert M. Stone (1 copy)

Lawrence Livermore Laboratory, P.O. Box 808, Livermore, CA 94550 - Attn: Dr. R.E. Kidder (1 copy)
Dr. E. Teller (1 copy)
Dr. Joe Fleck (1 copy)

Los Alamos Scientific Laboratory, P.O. Box 1663, Los Alamos, NM 87544 - Attn: Dr. Keith Boyer (1 copy)

Lulejian and Associates, Inc., Del Amo Financial Center, 21515 Hawthorne Blvd. - Suite 500, Torrance, CA 90503 (1 copy)

Lockheed Palo Alto Res. Lab., 3251 Hanover St., Palo Alto, CA 94303 - Attn: L.R. Lunsford, Orgn. 52-24, Bldg. 201 (1 copy)

Mathematical Sciences Northwest, Inc., P.O. Box 1887, Bellevue, WN 98009 - Attn: Dr. Abraham Hertzberg (1 copy)

Martin Marietta Corp., P.O. Box 179, Mail Station 0471, Denver, CO 80201 - Attn: Mr. Stewart Chapin (1 copy)

Massachusetts Institute of Technology, Lincoln Laboratory, P.O. Box 73, Lexington, MA 02173 - Attn: Dr. S. Edelberg (1 copy)
Dr. L.C. Marquet (1 copy)

McDonnell Douglas Astronautics Co., 5301 Bolsa Avenue, Huntington Beach, CA 92647 - Attn: Mr. P.L. Klevatt, Dept. A3-830-BBFO, M/S 9 (1 copy)

McDonnell Douglas Research Labs., Dept. 220, Box 516, St. Louis, MO 63166 - Attn: Dr. D.P. Ames (1 copy)

MITRE Corp., P.O. Box 208, Bedford, MA 01730 - Attn: Mr. A.C. Cron (1 copy)

North American Rockwell Corp., Autonetics Div., Anaheim, CA 92803 - Attn: Mr. T.T. Kumagi, C/476 Mail Code HA18 (1 copy)

Northrop Corp., 3401 West Broadway, Hawthorne, CA 90250 - Attn: Dr. Gerard Hasserjian, Laser Systems Dept. (1 copy)

Dr. Anthony N. Pirri, Physical Sciences, Inc., 18 Lakeside Office Park, Wakefield, MA 01880 (1 copy)

RAND Corp., 1700 Main Street, Santa Monica, CA 90406 - Attn: Dr. C.R. Culp/Mr. G.A. Carter (1 copy)

Raytheon Co., 28 Seyon Street, Waltham, MA 02154 - Attn: Dr. F.A. Horrigan (Res. Div.) (1 copy)

Raytheon Co., Boston Post Road, Sudbury, MA 01776 - Attn: Dr. C. Sonnenschien (Equip. Div.) (1 copy)

Raytheon Co., Bedford Labs, Missile Systems Div., Bedford, MA 01730 - Attn: Dr. H.A. Mehlhorn (1 copy)

Riverside Research Institute, 80 West End Street, New York, NY 10023 - Attn: Dr. L.H. O'Neill (1 copy)
Dr. John Bose (1 copy)
(HPEGL Library) (1 copy)

R&D Associates, Inc., P.O. Box 3580, Santa Monica, CA 90431 - Attn: Dr. R.E. LeLevier (1 copy)

Rockwell International Corporation, Rocketdyne Division, Albuquerque District Office, 3636 Menaul Blvd., NE, Suite 211, Albuquerque, NM 87110 - Attn: C.K. Kraus, Mgr. (1 copy)

SANDIA Corp., P.O. Box 5800, Albuquerque, NM 87115 - Attn: Dr. Al Narath (1 copy)

Stanford Research Institute, Menlo Park, CA 94025 - Attn: Dr. F.T. Smith (1 copy)

Science Applications, Inc., 1911 N. Ft. Meyer Drive, Arlington, VA 22209 - Attn: L. Peckam (1 copy)

Science Applications, Inc., P.O. Box 328, Ann Arbor, MI 48103 - Attn: R.E. Meredith (1 copy)

Science Applications, Inc., 6 Preston Court, Bedford, MA 01703 - Attn: R. Greenberg (1 copy)

Science Applications, Inc., P.O. Box 2351, La Jolla, CA 92037 - Attn: Dr. John Asmus (1 copy)

Systems, Science and Software, P.O. Box 1620, La Jolla, CA 92037 - Attn: Alan F. Klein (1 copy)

Systems Consultants, Inc., 1050 31st Street, NW, Washington, D.C. 20007 - Attn: Dr. R.B. Keller (1 copy)

Thiokol Chemical Corp., WASATCH Division, P.O. Box 524, Brigham City, UT 84302 - Attn: Mr. J.E. Hansen (1 copy)

TRW Systems Group, One Space Park, Bldg. R-1, Rm. 1050, Redondo Beach, CA 90278 - Attn: Mr. Norman Campbell (1 copy)

United Technologies Research Center, 400 Main Street, East Hartford, CT 06108 - Attn: Mr. G.H. McLafferty (3 copies)

DISTRIBUTION LIST (Continued)

United Technologies Research Center, Pratt and Whitney Aircraft Div., Florida R&D Center, West Palm Beach, FL 33402 Attn: Dr. R.A. Schmidtke (1 copy)
Mr. Ed Pinsley (1 copy)

VARIAN Associates, EIMAC Division, 301 Industrial Way, San Carlos, CA 94070 - Attn: Mr. Jack Quinn (1 copy)

Vought Systems Division, LTV Aerospace Corp., P.O. Box 5907, Dallas, TX 75222 - Attn: Mr. F.G. Simpson, MS 254142 (1 copy)

Westinghouse Electric Corp., Defense and Space Center, Balt-Wash. International Airport - Box 746, Baltimore, MD 21203 - Attn: Mr. W.F. List (1 copy)

Westinghouse Research Labs., Beulah Road, Churchill Boro, Pittsburgh, PA 15235 - Attn: Dr. E.P. Riedel (1 copy)

United Technologies Research Center, East Hartford, CT 06108 - Attn: A.J. DeMaria (1 copy)

Airborne Instruments Laboratory, Walt Whitorian Road, Melville, NY 11746 - Attn: F. Pace (1 copy)

General Electric R&D Center, Schenectady, NY 12305 - Attn: Dr. Donald White (1 copy)

Cleveland State University, Cleveland, OH 44115 - Attn: Dean Jack Soules (1 copy)

EXXON Research and Engineering Co., P.O. Box 8, Linden, NJ 07036 - Attn: D. Grafstein (1 copy)

University of Maryland, Department of Physics and Astronomy, College Park, MD 20742 - Attn: D. Currie (1 copy)

Sylvania Electric Products, Inc., 100 Fergeson Drive, Mountain View, CA 94040 - Attn: L.M. Osterink (1 copy)

North American Rockwell Corp., Autonetics Division, 3370 Miraloma Avenue, Anaheim, CA 92803 - Attn: R. Gudmundsen (1 copy)

Massachusetts Institute of Technology, 77 Massachusetts Avenue, Cambridge, MA 02138 - Attn: Prof. A. Javan (1 copy)

Lockheed Missile & Space Co., Palo Alto Research Laboratories, Palo Alto, CA 94304 - Attn: Dr. R.C. Ohlman (1 copy)

ILC Laboratories, Inc., 164 Commercial Street, Sunnyvale, CA 94086 - Attn: L. Noble (1 copy)

University of Texas at Dallas, P.O. Box 30365, Dallas, TX 75230 - Attn: Prof. Carl B. Collins (1 copy)

Polytechnic Institute of New York, Rt. 110, Farmingdale, NY 11735 - Attn: Dr. William T. Walter (1 copy)